REPORT SERIES IN AEROSOL SCIENCE
N:O 196 (2017)

PHYSICAL PHASE TRANSITIONS OF SECONDARY ORGANIC AEROSOL PARTICLES

AKI PAJUNOJA

Department of Applied Physics
Faculty of Science and Forestry
University of Eastern Finland
Kuopio, Finland

Academic dissertation

To be presented, with the permission of the Faculty of Science and Forestry of the University of Eastern Finland, for public criticism in auditorium MD100, Yliopistonranta 1, on Thursday 27.4., 2017, at 12 o'clock noon.

Kuopio 2017

Author's Address: Department of Applied Physics
P.O. Box 1627
FI-70211 University of Eastern Finland
aki.pajunoja@gmail.com

Supervisors: Professor Annele Virtanen, Ph.D.
Department of Applied Physics
University of Eastern Finland

Professor Kari Lehtinen, Ph.D.
Department of Applied Physics
University of Eastern Finland

Docent Jorma Joutsensaari, Ph.D.
Department of Applied Physics
University of Eastern Finland

Reviewers: Katrianne Lehtipalo, Ph.D.
Paul Scherrer Institute
Villigen, Switzerland

Tomi Raatikainen, Ph.D.
Finnish Meteorological Institute
Helsinki, Finland

Opponent: Proferssor Johathan Reid, Ph.D.
School of Chemistry
University of Bristol, UK

ISBN 978-952-7091-76-0 (printed version)
ISSN 0784-3496
Helsinki 2017
Unigrafia Oy

ISBN 978-952-7091-77-7 (pdf version)
Kuopio 2017
Itä-Suomen Yliopiston verkkojulkaisut

Abbreviations

ABI	Aerosol Bounce Instrument
ABS	Ammonium bisulfate
ADRE	Aerosol Direct Radiative Effect
AMS	Aerosol Mass Spectrometer
AN	Ammonium Nitrate
AS	Ammonium Sulfate
BSOA	Biogenic Secondary Organic Aerosol
BSA	Bovine Serum Albumin
BC	Black Carbon
BF	Bounced Fraction
CO	Critical Orifice
CCN	Cloud Condensation Nuclei
CCNc	Cloud Condensation Nuclei counter
CE	Collectien Efficiency
CPC	Condensation Particle Counter
DMA	Differential Mobility Analyzer
DMPS	Differential Mobility Particle Sizer
DRH	Deliquescence Relative Humidity
DOS	Dimethyl Octyl Sebacate
EDB	Electrodynamic Balance
ELPI	Electrical Low Pressure Impactor
ELVOC	Extremely Low Volatility Organic Compound
ERH	Efflorescence Relative Humidity
FHH	Frankel-Halsey-Hill adsorption
GF	Growth Factor
HGF	Hygroscopic Growth Factor
HR	High Resolution
HTDMA	Hygroscopic Tandem Differential Mobility Analyzer
IPCC	International Panel for Climate Change
LVOC	Low Volatile Organic Compound
MFC	Mass Flow Controller
MOUDI	Micro-Orifice Uniform Deposit Impactor
NPF	New Particle Formation
OA	Organic Aerosol
O:C	Degree of oxidation, ratio of oxygen and carbon numbers
OH	Hydroxyl radical
OFR	Oxidation Flow Reactor
OPC	Optical Particle Counter

PAM	Potential Aerosol Mass flow reactor
PID	Proportional-integral-derivative controller
PM	Particulate Matter
POA	Primary Organic Aerosol
PSL	Polystyrene Latex
RH	Relative Humidity
RTC	Residence Time Chamber
SE	Stokes-Einstein relation
SEM	Scanning Electron Microscope
SMEAR	Station for Measuring Forest Ecosystem-Aerosol interaction
SOA	Secondary Organic Aerosol
SOAS	Southern Oxidant Aerosol Study
SOM	Secondary Organic Material
SVOC	Semi Volatile Organic Compound
TDMA	Tandem Differential Mobility Analyzer
TOA	Top of Atmosphere
ToF	Time-of-Flight
UV	Ultraviolet
VBS	Volatility Basis Set
VOC	Volatile Organic Compound

Acknowledgements

The research presented in this thesis was carried out at the Department of Applied Physics of the University of Eastern Finland, Kuopio. I acknowledge the head of the department Prof. Kari Lehtinen for providing me with the working facilities during my thesis work. I express my sincere gratitude to Prof. Douglas Worsnop and Prof. Jose Jimenez for making all the successful collaborations possible.

I also acknowledge Dr. Katrianne Lehtipalo and Dr. Tomi Raatikainen for reviewing this thesis.

I would like to sincerely thank Prof. Annele Virtanen, Prof. Kari Lehtinen, and Dr. Jorma Joutsensaari, for being excellent supervisors, encouraging me and showing interest towards my work. Above all I am grateful to the leader of our research group Prof. Annele Virtanen. I could not ask for a better supervisor, group leader, team player, co-author and truly inspiring person! Your guidance and support during my scientific career has been outstanding. Thank you also for involving me in the high-level international research collaborations.

I want to thank all the wonderful co-authors I have had honor to work with. Special thanks to superb Dr. Andrew Lambe for giving me huge support during and after the visit in Boston, Dr. Weiwei Hu for helping me with the Alabama data, Dr. Jussi Malila for sharing the comprehensive expertise related to thermodynamics, my former office mate Dr. Liqing Hao for helping me numerous times, and of course Dr. Jani Hakala for being a great workmate during the trips in Boston and Alabama. I want to acknowledge also my office mates Olli and Eetu for helping me keep my feet on the ground during the last two years.

I have enjoyed working in Kuopio in our research group and there are lots of great people making even greater science! Keep up the good work and remember to continue the scientifically colorful coffee breaks in the future.

Finally I want to thank the people giving me something else to think and experience during my academic career, my best friends, my family, and especially my beautiful wife, Maaret.

Physical phase transitions of secondary organic aerosol particles

Aki Petteri Pajunoja

University of Eastern Finland, 2017

Abstract

Aerosols – fine particulate matter in air – are not only important for human health but also for atmospheric processes such as cloud formation and scattering of the sunlight in the atmosphere. Natural forests are a significant source for particulate matter: they emit gaseous compounds that are transformed by chemical reactions into molecules that form secondary organic aerosols (SOA). The SOA particles are formed from thousands of different organic molecules in air but yet, only a minor fraction of the compounds in the SOA particles have been identified. While the impacting mechanisms of the particles' physical and chemical properties on Earth's radiation budget are well-known and accepted, the significances of these effects remain to be quantified.

This thesis focuses on investigating the physical properties of SOA particles: specifically, the phase state and hygroscopicity. The link between the physical properties and chemical composition of the SOA particles is investigated by applying novel instrumentation in both, laboratory and field studies. Hygroscopicity of atmospheric SOA particles has been widely studied previously but there has not been a method to quantify the viscosity nor diffusion limitations of the SOA particles. So far it has been assumed that atmospheric SOA is either in solid or liquid form in the atmosphere. Our findings which are based on particle bounce measurements suggest that the water uptake of SOA resembles that of solid surfaces until the humidity is high enough for dissolution to occur. This changes the general understanding of their interaction with water vapour directly affecting their ability to scatter sunlight. In terms of interaction of the SOA particles with organic vapors, we demonstrate that at atmospherically relevant RH, the viscosity of the α-pinene SOA particles, which are considered to be representative for biogenic SOA in monoterpene dominated environments, has a minor effect on the evaporation of the particles.

The findings presented in this thesis increase the understanding of one of the most relevant atmospheric processes involving organic dominated aerosols. We also demonstrate that the difference in SOA hygroscopic behaviour in sub- and supersaturated conditions can lead to clear effects in the direct aerosol forcing – highlighting the need to correct description of the process in atmospheric models. Obtaining closure across the full RH range is therefore a critical issue for accurate climate modelling.

Keywords: aerosol, organics, phase state, viscosity, hygroscopicity

List of publications

This PhD thesis consists of an introduction to the topic and results followed by four research papers which are cited according to their roman numerals. Papers I, II and IV are reprinted with permission from the publisher, and Paper III is reproduced under the Creative Commons Attribution 3.0 License.

Paper I Pajunoja, A., Malila, J., Hao, L., Joutsensaari, J., Lehtinen, K. E. and Virtanen, A.: Estimating the viscosity range of SOA particles based on their coalescence time, *Aerosol Science and Technology*, 48, i-iv, doi:10.1080/02786826.2013.870325, 2014.

Paper II Pajunoja, A., Lambe, A. T., Hakala, J., Rastak, N., Cummings, M. J., Brogan, J. F., Hao, L., Paramonov, M., Hong, J. and Prisle, N. L., Malila, J., Romakkaniemi, S., Lehtinen, K. E. J., Laaksonen, A., Kulmala, M., Massoli, P., Onasch, T. B., Donahue, N., Riipinen, I., Davidovits, P., Worsnop, D. G., Petäjä, T. and Virtanen, A.: Adsorptive uptake of water by semisolid secondary organic aerosols, *Geophysical Research Letters*, 42, 3063-3068, doi:10.1002/2015GL063142, 2015.

Paper III Pajunoja, A., Hu, W.W., Leong, Y.J., Taylor, N., Miettinen, P., Palm, B.B., Mikkonen, S., Collings, D. R., Jimenez, J.L., and Virtanen, A.: Phase state of ambient aerosol linked with water uptake and chemical aging in the Southeastern US, *Atmosheric Chemistry and Physics*, 16, 11163-11176, doi:10.5194/acp-16-11163-2016, 2016.

Paper IV Yli-Juuti, T., Pajunoja, A., Tikkanen, O-P., Buchholz, A., Faiola C., Väisänen O., Hao L., Kari E., Peräkylä O., Garmash O., Shiraiwa M., Ehn M., Lehtinen K., and Virtanen, A., Factors controlling the evaporation of secondary organic aerosol from α-pinene ozonolysis, *Geophysical Research Letters*, doi:10.1002/2016GL072364, 2017.

Contents

1. Introduction 9
   1.1 Atmospheric organic aerosols 11
   1.2 Aims and scope 12
2. The properties of aerosols that affect their behavior in the atmosphere 13
   2.1 Phase state and particle-phase diffusion 13
   2.2 Partitioning of vapors – volatility 17
   2.3 Interaction with water vapor – hygroscopicity 19
      2.3.1 Water uptake of water soluble particles 19
      2.3.2 Water uptake of solid insoluble particles 20
3. Experimental methods 22
   3.1 Phase state measurements 22
      3.1.1 Aerosol bounce instrument (ABI) 23
   3.2 Hygroscopicity, growth and shrinking measurements 27
      3.2.1 TDMA systems to measure growth or evaporation 28
      3.2.2 CCNc to measure cloud activation 32
   3.3 Laboratory and field measurements 32
   3.3.1 SOA generation in a laboratory 33
   3.3.2 Field measurements 34
4. Results and discussion 35
   4.1 Laboratory SOA particles 35
      4.1.1 Viscosity range of SOA particles at dry conditions 35
      4.1.2 Phase transition RH of SOA particles with varied composition 37
      4.1.3 Evaporation kinetics of α-pinene SOA particles 40
   4.2 Physical properties of SOA particles in the atmosphere 44
      4.2.1 Effect of extended oxidation on SOA phase state (SOAS study) 46
   4.3 Implications of the results 47
5. Author's contribution 50
6. Summary 51
   6.1 Future perspectives 52

References 53

1. Introduction

Atmospheric aerosol particles are ubiquitous in Earth's atmosphere (Jimenez et al. 2009), affecting global climate, visibility, Earth's energy budget, and human health (Pöschl et al. 2005). During their lifespan in the atmosphere, the particles form, grow and transform depending on the ambient conditions, and travel vertically and horizontally depending on weather conditions. The atmospheric aerosol population, typically consisting of $10^2 - 10^6$ particles in every cubic centimeter of air (Seinfeld and Pandis, 2006), interacts with surrounding reactive trace gas molecules round-the-clock by taking them in or giving them away, and transforms to the prevailing environmental conditions, namely temperature and relative humidity. They change their chemical and physical properties due to chemical aging, solar radiation (oxidative aging) and interaction with condensable vapors (Wang et al. 2015). This heterogeneous interaction influences both the distribution of reactive atmospheric gases and the size distribution and properties of the aerosol particles. Depending on the conditions and the origin of the particles, their composition, and especially their size, the journey during their lifetime in the atmosphere can be from seconds to weeks, and from meters to thousands of kilometers (Seinfeld and Pandis 2006).

Typically, the particle population in the atmosphere consists of a few size modes which can be approximated by lognormal number size distributions (Hinds, 2012). The smallest, nanometer-scale nucleation mode (Kulmala et al. 2004) particles (~3 – 20 nm) have the ability to penetrate into human lungs efficiently (Peters et al. 1997), but they do not scatter/absorb solar radiation so effectively due to their small optical size and short lifetime in the atmosphere (Hinds 2012). The impact of aerosols on incoming solar radiation is typically reported in radiative forcing [Wm^{-2}] on top of the atmosphere (TOA). Submicron particles (diameter < 1μm) are often, especially in urban areas, dominated in number by Aitken or accumulation mode particles (~20 – 90 nm and ~90 – 1000 nm, respectively). They are big enough to scatter and absorb sunlight, and the net effect of a single aerosol particle on radiative forcing can be described with its single scattering albedo (Seinfeld and Pandis 2006). However, the albedo is always compared to Earth's natural reflectivity, which makes the modeling somewhat challenging. For example, particles in the upper troposphere in the daytime can either have warming effect on the climate if they exist above optically thick cloud, or a cooling effect if they flow above absorbing forest. Also, the composition of the particles plays a role in scattering; while water-soluble salt particles scatter solar radiation back to space (producing a cooling effect), insoluble black carbon particles absorb it and trap the solar energy to the atmosphere (producing a warming effect) (Stocker et al. 2014). The scattering and absorption effects of aerosols represent their *direct effect* on the climate (i.e., radiative interaction). To affect Earth's energy budget in the most efficient way, particles need to grow large enough to start acting as cloud condensation nuclei (CCN), and thus have an *indirect effect* on the Earth's energy balance (Kulmala et al. 2004). After a possible vertical updraft in the atmosphere, the particles may be able to reach water supersaturation conditions, reach CCN size

range and eventually create a cloud. But again, the vertical distribution of particles, cloud droplets (size and concentration) and the type of clouds all need to be taken into account when considering their effects on Earth's total radiative forcing, and thus, the climate. The visibility effect of aerosol particles is dominated by particles in the same size range as the smallest cloud droplets (i.e., micrometers). The biggest, super-micron particles, belong to the coarse mode (particles of diameter greater than 2,5μm), and their number concentration in the atmosphere is small compared to other particle modes. However, in many regions they dominate the atmospheric particle population in mass.

Despite the fact that the size (Dusek et al. 2006) and the number of the particles are the main properties controlling the influence of particle population on climate, the other physical and chemical characteristics of the particles may change this classification dramatically. Optically, the particles can vary from totally black particles to fully transparent particles. Particles can also vary in reactivity and solubility. For instance, in cloud droplet activation, the most hygroscopic particles smaller than 50 nm can activate as CCN, while even 1μm particles do not activate if they are totally hydrophobic and insoluble. Partly because of this, the greatest absolute uncertainties in IPCC 2014 radiative forcing report are for aerosol effects (Pachauri et al. 2014, Stocker et al. 2014). This is why we need to broaden our understanding of the physical properties such as the hygroscopicity, the phase state, and the morphology of atmospheric aerosol particles.

One of the most important factors affecting ambient aerosol optical properties is the particulate water volume. The water uptake of ambient aerosols is widely studied for various submicron aerosol types. Svenningsson et al. (1992) found that atmospheric submicron particles clearly have a lower hygroscopicity than pure salt particles, and concluded that particles contain a major insoluble part. At that time, atmospheric particles were generally assumed to contain hygroscopic sea salt and/or sulfate. Saxena et al. (1995) highlighted the importance of organic fraction on the hygroscopicity of atmospheric aerosols. Recently, the hygroscopicity of the organic fraction of the particles has been described with model frameworks (Topping et al. 2005) and also with simplified models (Petters and Kreidenweis 2007). However, certain assumptions are made in the models about the phase state and solubility of the particles, which can lead to remarkable differences between the models and real ambient observations. Among others, general assumptions are: 1) the atmospheric aerosol particles consist of completely liquid material, 2) they are in a thermodynamic equilibrium with the surrounding gas-phase and 3) they are treated as an ideal solution. Similar assumptions are typically made in condensational growth models in general (Donahue et al. 2006). More recently, non-ideal physical properties have been taken into consideration in process modeling (Koop et al. 2011, Riipinen et al. 2011, Shiraiwa et al. 2011, Zaveri et al. 2014) and also in the recent microphysical modeling (Shrivastava et al. 2013, Scott et al. 2015).

The assumptions listed above were questioned after the first direct observational evidence on the particle phase state from field measurements, which implied that ambient organic aerosols could be highly viscous or even glassy (Virtanen et al. 2010). A couple of years before that, Zobrist et al. (2008) had highlighted that atmospheric organic aerosols could form glasses, but their results were based on a laboratory study. A wholly new emphasis in science, with respect to ambient organic aerosol

properties, was awoken, leading to a great number of high profile research publications (e.g., Shiraiwa et al. 2011; Vaden et al. 2011; Kuwata et al. 2012, Riipinen et al. 2012; Renbaum-Wolff et al. 2013; Bateman et al. 2016). The experimentalists tried to find a way to measure viscosity of the particles and the modelers discussed the potential resultant consequences. Recent studies show that, indeed, the total number of particles (Riipinen et al. 2011), reactivity (Shiraiwa et al. 2011, Kuwata and Martin et al. 2012), photochemistry (Lignell et al. 2014), growth (Shiraiwa et al. 2013), water uptake, and timescales (Koop et al. 2011) of the processes may be dramatically affected by the non-liquid state of the atmospheric organic aerosol particles. However, an accurate viscosity estimation for different species existing in various places in the atmosphere is still lacking.

1.1 Atmospheric organic aerosols

Atmospheric aerosols are typically classified by their origin, formation process and composition (Friedlander 2000). Human-induced particles and gas-phase emissions are classified as anthropogenic emissions, while emissions from natural sources are named as biogenic emissions. Particles that are emitted directly to the atmosphere are called primary particles, and they typically exist in coarse mode. The main sources of primary particles in the atmosphere are the Earth's ground abrasion (desert dust, road dust), sea-spray formation, biomass burning (forest fires, anthropogenic) and exhaust processes (volcanic eruption, combustion, industrial) (e.g., McCormick et al., 1995). Until the early 1950s, primary particles were considered to be the only source for atmospheric aerosols (Went, 1960). The research of particles formed from the oxidation products of organic gas-phase precursors in the atmosphere started in the 1980s and such particles were named secondary organic aerosols (SOA). By contrast, primary particles composed mainly of organic species are named Primary Organic Aerosols (POA), which can act as seed particles for SOA material (Pohlker et al. 2012).

The formation of SOA particles occurs when supersaturated vapors do not reach any condensation surfaces, but they need to form clusters in order to maintain thermodynamic equilibrium (Kanakidou et al. 2005). In the next formation step, nucleation takes place: molecules with favorable vapor pressure and stickiness are trapped by the clusters, and early-stage nanoparticles are formed (Kulmala et al. 2004). The formation of nucleation mode particles starts from particle sizes of around 1.5 nm (Kulmala et al. 2007, Lehtipalo et al. 2010). When the probability that the molecules will stay in the condensed phase, is high enough, the stable particles continue to grow by condensation towards the accumulation mode, eventually reaching CCN size range (Kerminen et al. 2005). Organic aerosols are subject to chemical reactions with trace gases such as ozone (Shiraiwa et al. 2011), ammonia (Kuwata and Martin, 2012), nitrate (Kroll et al. 2011) or hydroxyl radical (Shiraiwa et al. 2012; Frosch et al. 2012). All can have an impact on the chemical composition (Wang et al. 2015) and particle size distribution (Shiwaiwa et al. 2013), and hence influence the physical properties of the particles (i.e., hygroscopicity (Kanakidou et al. 2005; Lambe et al. 2011), viscosity (Saukko et al. 2012), and radiative properties (e.g., Zaveri et al. 2012)). If the particles are formed by the oxidation of biogenic volatile organic compound (VOC) molecules (Hallquist et al. 2009), and by the condensation of their oxidation products varying from semivolatile organic compounds (SVOC) to extremely low volatile organic compounds (ELVOC), they are classified as Biogenic SOA (BSOA) particles (Poschl et al. 2010).

Anthropogenic SOA (ASOA) particles are formed from anthropogenic precursors instead. Nearly 50% of the observed aerosols in the troposphere are estimated to originate from secondary aerosol formation processes (Spracklen et al. 2010).

Despite their small size, SOA particles contribute a major mass fraction (20-90%) of the submicron (<1μm) particles in the atmosphere (Jimenez et al. 2009). The substantial role of BSOA particles in the global climate comes from their ability to act as CCN and directly scatter solar radiation (Ramanathan et al. 2001), while ASOA particles are typically associated with severe health effects (Hallquist et al. 2009). In urban areas, SOA particles can be formed from a mixture of biogenic and anthropogenic gas-phase products, or SOA particles can stick together (i.e., coagulate) in the atmosphere to form chain-like particles or agglomerates. It is also possible that biogenic oxidation products can condense on pre-existing anthropogenic aerosol particles and, thus, change their behavior in the atmosphere. If the population consists of particles of different compositions, the population is called externally mixed aerosol. Correspondingly, the particle population consisting only of similar aerosol particles is named as internally mixed aerosol.

BVOCs are much more abundant in the atmosphere than anthropogenic VOCs, and tens of thousands of VOCs have been measured in the atmosphere (Guenther et al. 2012). Forests are one of the main sources of global organic aerosols and different types of trees emit different VOC mixtures (Xu et al. 2015). Atmospheric SOA particles are often formed from their oxidation products, but only a minor part (~10%) of them is yet reported (Kanakidou et al. 2005; Ehn et al. 2014). Even if we were able to map all of the compounds existing in the particle phase, the information could not be utilized in climate models without significant simplification, due to limitations in computational time. The same challenge also holds for particle properties. However, by increasing our understanding of the species and actual physical processes of the SOA particles, we are able to rely on scientifically quantified principles when defining the revised, usable and proper simplifications.

1.2 Aims and scope

This thesis focuses on aerosol particles that consist of secondary organic material. The main objective of the study is to increase our understanding about the physical properties of SOA particles: namely, the phase state and hygroscopicity. We aim to provide more information on the phase state of the SOA particles with improved and novel equipment. The phase state of particles has an effect on the other properties of the particles, but is this significant when considering the effects on the climate? Is it the composition of SOA particles that has relevance for the climate through its effect on particle size, or its effect on the ability to take up water? To answer these questions and meet the goals of our study, this thesis is designed to include the following steps:

1) Quantify the viscosity range for SOA particles (**Paper I**).
2) Build an improved tool which measures the particle bounce of both laboratory-generated and atmospheric SOA particles to investigate their phase state at wide RH range (**Papers II, III**).

3) Investigate the effect of particle phase on water uptake, cloud activation, evaporation, chemical aging, and morphological changes (**Papers II, III, IV**).
4) Study the dependence of the particle phase state on hygroscopicity and the degree of oxidation of the particles (**Papers II, III**).

2. The properties of aerosols that affect their behavior in the atmosphere

SOA particles result from the need of individual atmospheric molecules to undergo energy state change from the gas phase (i.e., negligible binding energy between the molecules) to the solid (i.e., specific molecular order due to intermolecular forces) or liquid (i.e., molecules bonded loosely together) phase state. The vapor pressure of the condensing/evaporating compound controls the gas-to-particle interaction; molecules with higher vapor pressure in the gas phase than on the surface of the SOA particles are more likely to be trapped on the surface layer (adsorption) of the particles. After the surface accommodation, the molecules are able to diffuse through the surface into the bulk of the particles (absorption). Bidirectional partitioning continuously affects the concentrations of species (e.g., water and organics) existing in the particle phase, in order to retain thermodynamic equilibrium. Partitioning, which depends on particle volatility, also controls the rates and mechanisms of oxidative aging reactions and the amount of oxidized organic aerosol (Donahue et al. 2012). Understanding the interfacial mass transport process also requires knowledge about the phase state and composition of the particle bulk material (Koop et al. 2011). In liquids, even the biggest organic molecules diffuse unrestrictedly, whereas in glassy solid matter, the motion of diffusing molecules may be kinetically hindered. Thus, the phase state of particle bulk material can affect particle growth and reactivity, which then influences the number, size, morphology, and composition of the particle population (Riipinen et al. 2011, Shiraiwa et al. 2013; Shrisvastava et al. 2013, Zaveri et al. 2014). The affinity of particles for water is represented by their hygroscopicity. Hygroscopicity describes the ability of the particles to attract and hold water vapor. A few of the most relevant properties of the SOA particles, related to the aerosol processes that play key roles in the atmosphere, are summarized in following chapter. Those are 1) the phase state of the SOA particles, 2) the volatility of the organics which contribute to the SOA formation, and 3) the hygroscopicity of the SOA particles.

2.1 Phase state and particle-phase diffusion

Based on recent studies, atmospheric aerosol particles can consist of completely liquid, amorphous semisolid, crystalline or glassy solid material (Zobrist et al. 2008, Virtanen et al. 2010, Power et al. 2013, Renbaum-Wolff et al. 2013, Bateman et al. 2016). Crystalline species, such as typical inorganic salts (ammonium sulfate, sodium chloride etc.), have their characteristic deliquescence RH (DRH), where they suddenly change their phase state from a crystalline structure into a liquid form. As the wetted particles are dried again, they stay liquid until RH is lower than the characteristic efflorescence RH (ERH) of the particles. Below ERH, the particles lose all of the

particle-phase water and change rapidly back to the crystalline solid phase state (Saukko et al. 2012). Both DRH and ERH are specific to every crystalline substance, but particle size (Swietlicki et al. 2008) and condensed organics also affect the ERH and DRH of well-known inorganic salts (Smith et al. 2012, Shiraiwa et al. 2013).

Whether material is liquid, solid, or in an intermediate form (i.e. semisolid), can be described by its dynamic viscosity, η. Viscosity represents the materials' ability to resist structural deformation under mechanical stress. A typical viscosity categorization is shown in Fig. 2.1. A liquid state has been proposed to be at a viscosity range of $\eta < 10^2$ Pa s, whereas a solid phase state has proposed to be at $\eta > 10^{12}$ Pa s (Koop et al. 2011). Materials changing their viscosity as a function of RH and/or *T,* without rapid phase changes, are referred to as amorphous materials. Amorphous materials lack long-range molecular order, whereas in crystalline substances strict order exists. An amorphous solid is defined as a glassy solid phase state, $\eta > 10^{12}$ Pa s. Glass transition is a characteristic reversible transition of a substance from a glassy state into a molten/amorphous state, and it occurs at certain *T*. While crystalline substances have their characteristic melting temperature, amorphous substances have their characteristic glass transition temperature. In amorphous water-soluble materials, water can act as a plasticizer for SOA material (Zobrist et al. 2011), leading to a decrease in solidness at a higher RH until the water content is high enough to reach the liquid viscosity range, i.e., $\eta < 10^2$ Pa s (Shiraiwa et al. 2013). Recently, atmospheric SOA particles have shown to be composed of amorphous materials, changing their viscosity from solid to liquid depending on particle composition and the prevailing *T* and RH (Koop et al. 2011, Shiraiwa et al. 2011, Virtanen et al. 2010). Accordingly, particle-phase diffusion of trace gases has been shown to decrease in the SOA particles, especially at dry and/or cold conditions (Abramson et al. 2013, Tong et al. 2011, Price et al. 2014).

The viscosity of atmospheric SOA particles determines whether the gas-to-particle interaction is confined to the surface region of the particles (adsorption) or is able to proceed in the interior of the particles (Shiraiwa et al. 2011). The diffusion of molecules in the SOA is, thus, linked to viscosity of the SOA, as described in the earlier section. With high enough viscosity, the vapor uptake can be limited by the amorphous solid structure of the SOA particles, and the condensing molecules may stay on the surface rather than diffusing into the core of the SOA particles. Thus, the diffusion mixing beyond the particle surface may be remarkably delayed (Shiraiwa et al. 2013). The vast majority of the current models assume a liquid phase state, and hence the fast particle-phase mixing. In this case, slow particle phase mixing can lead to fault predictions of the particle number concentration (Riipinen et al. 2011), particle size distribution (Zaveri et al. 2014), chemical reactivity (Shiraiwa et al. 2011), gas-phase and particle mass concentrations (Shiraiwa and Seinfeld 2012), particle diameters (Shiraiwa et al. 2013), and ice-nucleation ability (Berkemeier et al. 2014).

The diffusion coefficient describes the ability of the molecules to penetrate through material. The most common modeling framework is the Stokes-Einstein (SE) relation, which can be used to estimate the diffusion coefficient of compound *i* as (Seinfeld and Pandis, 2006)

$$D_i = \frac{k_B T}{6\pi r_i \eta} \quad (1)$$

where T is the temperature, η is particle-phase viscosity, r_i is the radius of the diffusing molecule, and k_B is the Boltzmann constant. The SE relation is designed to describe the diffusion of molecules in a bulk phase consisting of similar molecules (i.e., self-diffusing). The time-dependent diffusion of water molecules in a spherical volume (i.e., inside the particle) can be calculated as (Shiraiwa et al. 2011)

$$D_i = \frac{d_p^2}{4\pi^2 t_{\mathrm{mix,i}}} \quad (2)$$

where d_p is the particle diameter and $t_{\mathrm{mix,i}}$ is the time for molecules i to penetrate from the particle surface into the core of the particles (i.e., *mixing time*). Here, D_i is assumed to be uniform throughout the particle volume. By combining these two equations, we get a relationship between mixing time and particle viscosity as:

$$t_{\mathrm{mix}} = \frac{3 r_i d_p^2}{2\pi k_B T}\eta. \quad (3)$$

These diffusion equations are based on the SE relation, which is valid when we are far above glass transition T (i.e., low enough viscosity), and when the diffusing molecules are within the size range of the molecules in the bulk. However, the radius of a water molecule is approx. 0.14 nm (Sorjamaa and Laaksonen, 2007), whereas the radius of typical low-volatility organic oxidation product of α-pinene ozonolysis is around 1 nm (Ehn et al. 2014). The difference in size between the diffusing water molecule and surrounding solid phase organics increases the resulting diffusion coefficient compared to the values estimated with eq(1) and eq(2). Hence, in this case, the mixing times are clearly shortened. Multiple studies have highlighted the SE relation to be valid only in dilute conditions where the interactions between differently sized molecules are diminished. The relationship of the mixing time and viscosity is illustrated in Fig. 2.1 for 1 nm – 10 μm SOA particles, and for 1 nm diffusing organic oligomers (single molecule). For water molecules and other small molecules (e.g., ozone, O_3), the effective mixing time in semisolid and solid 100 nm particles is much faster than the mixing times for organic oligomers (Shiraiwa et al. 2013), leading to the possibility that water will mix into the particle-phase but the organic compounds stay on the surface of the particles. This may lead to gradient in chemical composition and hence reactivity in the particle-phase. Zobrist et al. (2011) estimated the diffusion coefficient for water to be ~10^{-12} cm^2 s^{-1} at glass transition T of sucrose particles while the self-diffusion (eq(1), see x axis in Fig. 2.1.) would give a value around 10^{-19} – 10^{-20} cm^2 s^{-1}. Tong et al. (2012) studied mixing times of water in glassy sucrose particles (diameter of 100 nm) at room T instead, and reported a scale of 10 – 100 s, which is significantly shorter than the SE relation would predict (i.e., > 10000 s).

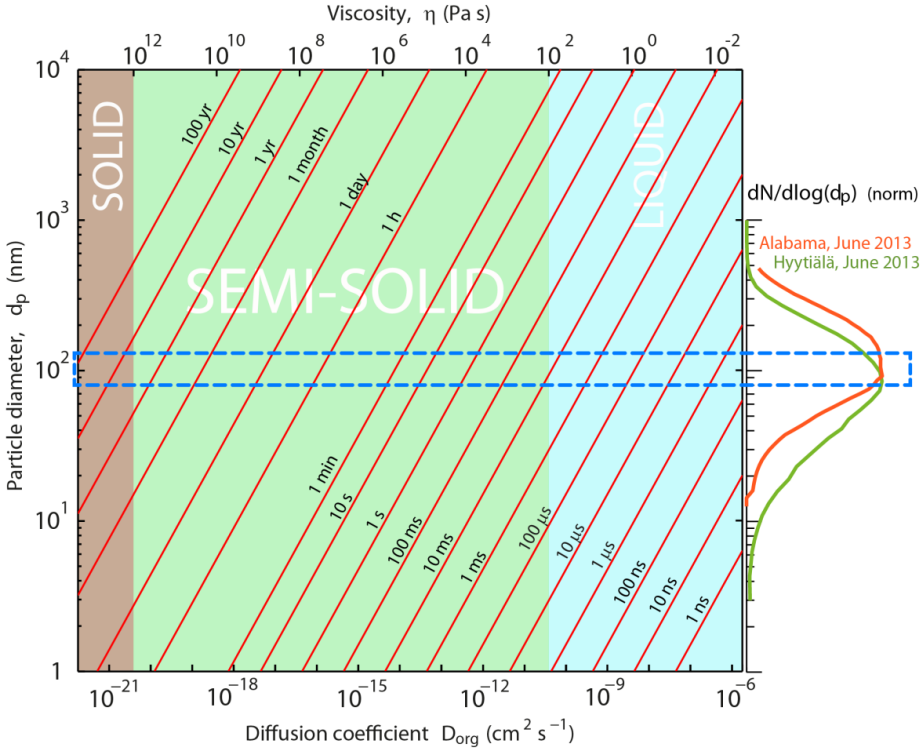

Figure 2.1. | Viscosity vs. diffusion. The relationship between particle diameter (d_p, y axis), particle dynamic viscosity (η, top axis and background color), diffusion mixing time ($t_{mix,org}$, red lines), and diffusion coefficient for typical organic oxidation product of α-pinene ozonolysis calculated with equation (2) (D_{org}, bottom axis). The dashed blue box illustrates the size range of the SOA particles studied in this thesis (i.e., 80 – 120 nm). Other parameters used in the equations are: T = 298 K, r_i = $5 \cdot 10^{-10}$ m, k_B = $1.38065 \cdot 10^{-23}$ J K^{-1}. In addition, campaign median number size distributions from ambient observations adapted from **Paper II** and **III** are shown on the right hand side (green and red bell-shaped curves, respectively).

Coalescence theory. Depending on the particle formation and growth conditions, SOA particles can coagulate together and form chain-like particles or agglomerates. The shape of the formed agglomerate changes in time depending on its viscosity: near-liquid agglomerates swell into a spherical structure within a millisecond, whereas highly viscous solid agglomerates can exist in a non-spherical state for months. This structural change from an aspherical to spherical shape is named as coalescence. Coalescence can be easily illustrated by combining two honey droplets together on a plate: due to the semisolid phase state of honey, the swelling of the droplets takes few minutes. It is driven by the minimization of surface energy (and area) of the particles. Frenkel et al. (1945) introduced a

coalescence theory for small particles which are consisted of two equal-sized and spherical primary particles. For coalescing these particles together, the coalescence relaxation time, τ_{coal}, can be estimated as (Frenkel et al. 1945)

$$\tau_{\mathrm{coal}} = \frac{d_{\mathrm{p}}}{\sigma}\eta \quad (4)$$

where d_{p} is the diameter of the primary particle, η is particle-phase viscosity, and σ is the surface tension of the particles. This simple linear relationship between particle viscosity and coalescence time can be indirectly used to quantify viscosity range for SOA particles. It has been recently used in, e.g., **Paper I**, Price et al. (2014), Zhang et al. (2015), Järvinen et al. (2015) for SOA particles.

2.2 Partitioning of vapors – volatility

Gas-phase molecules bombard the surfaces of the aerosol particles continuously. At typical ambient pressure and temperature (1013mbar and 25°C), air consists of around $2.7 \cdot 10^{19}$ individual molecules every cubic centimeter, leading to a mean free path of 68 nanometers between collisions (Hinds, 2012). Depending on molecules' characteristic saturation vapor pressures, they can condensate into or evaporate from the particles. In principal, volatility is controlled by the vaporization enthalpy of the compound over a liquid surface. If the particle-phase is thought to be an ideal solution, the equilibrium vapor pressure of compound *i* over the curved surface of an aqueous aerosol particle is (Seinfeld and Pandis 2006)

$$p_{\mathrm{eq,i}} = x_{\mathrm{i}} p_{\mathrm{sat,i}} \mathrm{Ke} \quad (5)$$

where $p_{\mathrm{sat,i}}$ is the saturation vapor pressure of compound *i* over a flat pure liquid surface, and x_{i} is the mole fraction of compound *i* in the particle, and Ke is a Kelvin curvature term. For a flat surface, the simplest example is a definition of relative humidity, RH:

$$p_{\mathrm{eq,water}} = \frac{\mathrm{RH}}{100\%} p_{\mathrm{sat,water}} \quad (6)$$

In other words, the general particle-phase effect of a solute is to decrease the equilibrium partial pressure of a species from the equilibrium vapor pressure of the pure species. In an ideal solution, this fractional decrease equals the mole fraction in the condensed phase. Particle curvature changes the equilibrium vapor pressure of species in the particle phase, especially at the sub-50 nm particle size range. Vapor pressure over a curved surface, like the aerosol particle, is linked to the diameter of a droplet with the Kelvin equation (Thomson 1871) as

$$\mathrm{Ke} = e^{\frac{4\sigma V}{dRT}} \quad (7)$$

where σ (N m^{-1}) is the surface tension, R (J mol^{-1} K^{-1}) is universal gas constant, T (K) is temperature, d (m) is the diameter of the droplet, and V (m^3 mol^{-1}) is the droplet molar volume. The flux of molecules condensing to the particle phase can be described by the *condensation equation*, and the resulting change in particle diameter over time is (Seinfeld and Pandis 2006)

$$\frac{dd_p}{dt} = \frac{4D_i M_i}{RTd_p\rho_p} f(Kn, \alpha)(p_i - p_{eq,i}) \quad (8)$$

where D_i is the diffusion coefficient for species i in air, M_i is its molecular weight, and f(Kn, α) is the transition regime correction factor for mass transport. This approach is used in **Paper IV**.

Only a small fraction of all organic compounds in the atmosphere have the ability to stay in/on the particle. This particular property is a low enough volatility, and the majority of the atmospheric compounds require chemical transformation to reach that low volatility range (Donahue et al. 2006). Typical precursor gases for SOA particles are VOCs, which require a significantly higher vapor mass concentration to be condensed than observed anywhere in the atmosphere. Chemical aging (oxidation) provides a way for VOCs to decrease their volatility so that they start to condense on the particles. In terms of the mass concentration of total condensed organic molecules, C_{OA}, and the saturation mass concentration of the compound i, C_i^*, the partitioning coefficient of the compound i at a steady state can be derived from (Donahue et al. 2006)

$$\xi_i = \left(1 + \frac{C_i^*}{C_{OA}}\right)^{-1};\ C_{OA} = \sum_i C_i \xi_i \quad (9)$$

where ξ_i is a fraction of volatility bin i in the particulate phase. If $C_i^* = C_{OA}$, the species i will be 50% in the particle-phase at equilibrium ($\xi_i = 0.5$). With this semi-empirical equation, we are able to estimate a fraction of the compound i existing in the condensed phase if the total OA concentration is known and the typical logarithmically distributed volatility bins introduced in Donahue et al. (2006), are employed. This is a basic principle of 1-dimensional *Volatility Basis Set* (VBS). It describes organic aerosols by separating low volatility compounds into $\log_{10}$ -spaced bins of C^* which are proportional to the saturation vapor pressures of the compounds. Originally, the VBS is designed to contain a volatility range of semi volatile organic carbon molecules (SVOCs, $10^{-0.5}$ – 10^3 μg/cm^3), meaning saturation concentrations between $10^{-0.5}$ and 1000 micrograms per cubic centimeter. Recently, less volatile categories such as low volatile (LVOCs, $10^{-4.5}$ – $10^{-0.5}$ μg/cm^3) and extremely low volatile OCs (ELVOCs, 10^{-20} – $10^{-4.5}$ μg/cm^3) have been shown to exist in the SOA particle-phase (Ehn et al. 2014), expanding the VBS presentation to much lower vapor pressures.

VBS bins can be used to describe the composition and evaporation of OA, and the evaporation of each bin can be calculated analogously with eq(8), and thus we get the mass transfer of the particle from

$$\frac{dm_p}{dt} = \sum_{i=1}^{n} J_i \quad (10)$$

where n is the number of VBS bins, and J_i is the change in the concentration of bin i (corresponding to C_i). The gas-particle partitioning of organic compounds is sensitive to temperature and its effect has typically taken into account by using the Clasius-Clapeyron equation (Donahue et al. 2006). Recently, VBS was also extended to contain elemental carbon and oxygen numbers and to link the degree of oxidation of SOA particles to the saturation concentrations of the species of OA (Donahue et al. 2011, Donahue et al. 2012).

Evaporation modelling. In **Paper IV**, we simulate an evaporation of SOA particles using two models. One model assumes well-mixed liquid-like particles, while the other, the Kinetic multi-layer model for

gas-particle interactions in aerosols and clouds (KM-GAP), can simulate the evaporation of semisolid SOA particles (Shiraiwa et al. 2012). In KM-GAP, the particle is divided into layers; as the condensed compounds with the highest volatility start to evaporate from the outmost layer (surface), these compounds start to diffuse from the bulk layers towards the surface layer (due to gradient in concentrations between the layers). Here, the particle viscosity (η) is assumed to be composition dependent, and it is calculated according to

$$\log_{10}\eta = \sum_{i=1}^{n} x_i \log_{10}(b_i) \quad (11)$$

where x_i is the molar fraction of the volatility bin i representing dry particles, and b_i is a parameter describing how the fraction of the compounds included in bin i contribute to the total viscosity of the particle. In both models, eight VBS bins were chosen to represent the studied SOA mass.

2.3 Interaction with water vapor – hygroscopicity

2.3.1 Water uptake of water soluble particles

SOA particles interact continuously with the surrounding gas-phase molecules and transform to the prevailing environment conditions by absorbing water and growing in size. Atmospheric conditions may cover the full range of RH, with typical values ranging from 20% to 100% in the planetary boundary layer (Martin, 2000). Water is an abundant atmospheric constituent which is present in the particle phase as a function of RH, T, aerosol number distribution, chemical composition, and physical structure. It can easily double the size of the particles and/or change their light-absorptivity and, thus, change their climate effect. The conditions needed for aqueous water droplets to be in equilibrium with gas-phase water vapor can be described according to Köhler theory (Köhler 1936). It states that the water vapor saturation ratio equals water activity, a_w, times Kelvin term (eq(7)). Raoult's law instead states for ideal solutions that the vapor pressure of solution ($p_{solution}$) above the particle is equal to the vapor pressure of the pure water (p^0_w), scaled by the mole fraction of the water present, x_w. In other words, water activity equals mole fraction of water in an ideal water solution, and it can be calculated as

$$a_w = x_w = \frac{V_w\rho_w/M_w}{V_w\rho_w/M_w + V_s\rho_s/M_s} \quad (12)$$

V_s, ρ_s and M_s are volume, density and molar mass of the solute, respectively, and subindex w refers to water. This equation assumes volume additivity. Raoult's law works pretty well for dilute solutions due to the effective attraction between water and solute molecules not being that dominant. If the concentration of solute molecules increases and the attraction between the solute and water molecules differs from the force between two water molecules, the equilibrium is not ideal, and thus needs to be corrected. A common way to correct non-ideal mixing effects between water molecules and the dissolved molecules in the mixture is to use water activity coefficient Γ_w in Raoult's law as

$$a_w = x_w\Gamma_w \quad (13)$$

However, in this thesis, water activity coefficient, Γ_w, was assumed to be 1 (if not otherwise noted). Both Kelvin equation (eq(7) and Raoult's law can be combined by using their termed form and hence giving an equation for saturation ratio of water:

$$S = \mathrm{RH}/100\% = x_w e^{\frac{4\sigma V}{dRT}} \quad (14)$$

which basically is Köhler-theory, but the water activity is represented with the mole fraction of water, x_w. The water content of aerosol particles can be calculated based on this equation for the entire particle size range and RH range. In a case of SOA particles, an average molecular weight and density of the mixture of organic species needs to be used in eq(12). This was the initial approach to calculate the water content of the SOA particles in **Papers II-IV,** and the principle was applied with the following methods in **Papers III** and **IV**.

***κ*-Köhler theory**. Hygroscopicity studies of atmospheric aerosol particles were driven by the need for climate models to predict the effect of particles' abilities to take up water on radiative forcing. These models could not use complicated hygroscopicity theories; a much simpler approach was desired. Therefore, Petters and Kreidenweis 2007 proposed a new parametrization for water uptake and introduced a single hygroscopicity parameter *κ*. The theory rests on eq(12), but the relationship between water activity, a_w, and *κ* is written as (Petters and Kreidenweis 2007)

$$\frac{1}{a_w} = 1 + \kappa \frac{V_s}{V_w} \quad (15)$$

where V_s is the volume of the water-soluble solute and V_w is the volume of the particulate water. By applying Zdanovskii, Stokes, and Robinson's (ZSR) assumption and assuming Raoult's law, they defined *κ–Köhler theory* over the whole RH range as (Petters and Kreidenweis 2007)

$$S = \frac{d^3 - d_{\mathrm{dry}}^3}{d^3 - d_{\mathrm{dry}}^3(1-\kappa)} e^{\frac{4\sigma_s M_w}{dRT\rho_w}} \quad (16)$$

where d is a diameter of the wet droplet, d_{dry} is a particle dry diameter, and ρ_w is the density of pure water. The basic idea of the theory is that a single value for *κ* can be used for each aerosol type of an aerosol population. The approach has been shown to be valid for sea salt and other highly water soluble compounds. However, their study invoked the "SOA research community" to test the parametrization for various ambient and laboratory SOA, which opened plenty of new research questions. Later, *κ–Köhler theory* turned out a handy comparison theory for non-ideal water uptake cases. In this thesis, FHH adsorption isotherm (see the next Sect.) is the studied water uptake process for insoluble, but water active, particles.

2.3.2 Water uptake of solid insoluble particles

If the particles are semisolid/solid and insoluble in water, they cannot be treated as water solutions, and thus, the solution theories (e.g., Raoult's law) are not valid. The insoluble particles can take up water on their surface if the surface layer is water active (hydrophilic) and not hydrophobic. This water uptake mechanism is called an adsorption. The adsorptive water uptake is a well-known water uptake mechanism for insoluble dust particles (Sorjamaa and Laaksonen, 2007).

FHH adsorption. One scenario for the non-ideal water uptake of SOA particles is the adsorption which is utilized in **Paper II**. SOA particles have been shown to be in an amorphous solid phase state, which proves that the particles cannot be dissolved into water at that RH range, and thus, they cannot be considered as an ideal solution. The original Raoult's law can be used only if the particles are completely soluble and dilute. Sorjamaa and Laaksonen (2007) used the multilayer adsorption theory by Frenkel, Halsey and Hill (FHH, Frenkel, 1955; Halsey, 1948; Hill, 1949) in modeling the cloud condensation nuclei (CCN) activation of insoluble submicron particles, and recently it has been used in several studies (Kumar et al. 2009, Kumar et al. 2011a, Kumar et al. 2011b, Laaksonen et al. 2016). FHH theory is based on dispersion forces being the dominant attractive interaction between the particle surface and the adsorption layer. The substance needs to be hydrophilic and thus, attractive for the water molecules, but the condensed water layers stay on the top of the particles due to the insoluble (or sparingly soluble) and dense bulk material. The thickness (θ, number of water monolayers) of the water layer can be fitted to experimental data with fitting parameters A_{FHH} and B_{FHH}, using the following equation:

$$\theta(\mathrm{RH}) = \left(\frac{A_{\mathrm{FHH}}}{\ln(\frac{100\%}{\mathrm{RH}})} \right)^{1/B_{\mathrm{FHH}}} . \quad (17)$$

For completely insoluble particles, it can then be added to the hygroscopic growth factor (GF; ratio between particle wet and dry diameters) equation as

$$\mathrm{GF}(\mathrm{RH}) = \frac{d_{\mathrm{dry}} + 2\theta(\mathrm{RH}) d_{w.\mathrm{layer}}}{d_{\mathrm{dry}}} \quad (18)$$

where $d_{\mathrm{w.layer}}$ = 0.28 nm is the thickness of one water layer (Sorjamaa and Laaksonen, 2007). Here, the adsorption is the only existing water uptake mechanism. In the case that particles consist both on the insoluble core and a water-soluble aqueous shell, eq(13) and eq(16) can be combined, as shown in Kumar et al. (2011), and we get equilibrium saturation ratio (S = RH/100%) for a wet particle containing an insoluble core as

$$\frac{\mathrm{RH}}{100\%} = x_{\mathrm{w}} e^{\frac{4\sigma_{\mathrm{w}} M_{\mathrm{w}}}{RT\rho_{\mathrm{w}} d_{\mathrm{dry}} \mathrm{GF}(\mathrm{RH})}} e^{-A_{\mathrm{FHH}}(\theta)^{-B_{\mathrm{FHH}}}} \quad (19)$$

The FHH-term can be added as a factor to eq(13). In the case that the particles are sparingly soluble with insoluble core diameter being d_{core}, a solute fraction in Raoult's term, x_{w}, can be modified according to estimations based on the measured GF(RH), where moles of water and solute can be written as

$$n_{\mathrm{w}} = \frac{\pi}{6} (\mathrm{GF}^3 - 1) d_{\mathrm{dry}}^3 \frac{\rho_{\mathrm{w}}}{M_{\mathrm{w}}} \quad (20)$$

and

$$n_{\mathrm{s}} = \frac{\pi}{6} \left(d_{\mathrm{dry}}^3 - d_{\mathrm{core}}^3 \right) \frac{\rho_{\mathrm{s}}}{M_{\mathrm{s}}}, \quad (21)$$

respectively. Here, V_{s}, ρ_{s} and M_{s} are the same as in eq(12), GF is the hygroscopic growth factor, d_{core} is the diameter of insoluble particle core, and d_{dry} is the initial dry diameter of the particles.

3. Experimental methods

The properties of aerosol particles are challenging to measure due to their small size and sometimes rapid physical and chemical changes. Offline methods, such as filter sampling, lack time resolution, whereas online methods sometimes struggle with a high enough signal-to-noise ratio. Particles can be measured directly but indirect measurements such as hygroscopicity, volatility, and phase state measurements are often used as a basis for composition analysis. Most of the time, aerosol particles exist in an equilibrium with the surrounding gas-phase, but this is not always the case. For instance, the phase state of the particles can be so glassy solid that the particle matrix itself limits the gas-to-particle interaction, which then may trap molecules to the particle-phase (Riipinen et al. 2011, Shiraiwa et al. 2011). This introduces a time-dependent behavior for the particles in the atmosphere, and in the measurement systems. In all aerosol measurement set-ups, these proposed artifacts need to be taken into account, and possibly checked with additional measurements.

The measurements conducted in this thesis work are based on earlier studies and instrument development. Particle composition is directly measured with aerosol mass spectrometer (Jayne et al. 2000; De Carlo et al. 2007), phase state and RH-induced phase transitions of the particles are measured with the aerosol bounce instrument (Saukko et al. 2012), hygroscopicity is investigated by analyzing the hygroscopic growth (Rader et al. 1986; McMurry et al. 1989) and cloud activation (Roberts and Nenes, 2005) of the humidified particles, while evaporation is studied by monitoring the particles' size reduction with time (Liu et al. 1978). In this chapter, a short overlook on the most common methods used to study the above-mentioned processes are given, and the specific methods used in this work are described in more detail. In addition, descriptions of the measurement campaigns performed both in the laboratory and in the field are given at the end of this chapter.

3.1 Phase state measurements

The phase state of aerosol particles can be qualitatively studied by investigating their physical properties. The phase state of SOA particles has been inferred from particle mechanical bounce measurements (**Paper II & III**, Bateman et al. 2014, Bateman et al. 2015; Bateman et al. 2016, Li et al. 2015, Saukko et al. 2012, Saukko et al. 2015, Virtanen et al. 2011, Virtanen et al. 2010) and bounce patterns (Kidd et al. 2014). A few direct viscosity measurement methods are also available, such as bead mobility technique (Renbaum-Wolff et al. 2013, Song et al. 2015), poke-and-flow (Grayson et al. 2015, Song et al. 2015), or shape change (**Paper I**, Zhang et al. 2015, Järvinen et al. 2016). The method used in Kidd et al. (2014) rests on the visual bounce pattern analysis of submicron particles; liquid particles do not bounce from the substrate but create a line-pattern, whereas semisolid/solid particles bounce at least once, and attach again to the plate next to the central line. They investigated 270 – 600 nm particles, whereas Renbaum-Wolff et al. (2013) and Grayson et al. (2015) studied super-micron 20-50μm particles consisting of SOM extracted from water solutions with their bead-mobility and poke-flow methods. In the bead-mobility method, a coarse single particle nebulized onto a hydrophobic slide is doped with nonreactive submicron melanine particles which are then optically tracked in the particle phase, as the surrounding flow has caused movements of the beads. This can be done in various RH. Bead speed changes linearly from 10^{-6} μm/ms to 10^{-1} μm/ms as the viscosity of the bulk particle

decreases from 10^3 to 10^{-3} Pa s, correspondingly. This calibration relationship was measured for sugars and other laboratory species, and was then conducted for SOM. The method is limited to viscosity values lower than 10^3 Pa s. In the poke-and-flow method, super-micron particles are generated in the same way as in bead-mobility measurements, but after the humidification they are poked with a needle. The time-dependent effect of poking on the deformation and recovery of the particle is again optically tracked, and the method can be used with semisolid substances with viscosity values up to 10^6 Pa s. Particle morphology and coalescence theory was used as an indicator for viscosity of SOA particles in **Paper I**. The particles were collected on a TEM filter, which was then stored in a dry and dark place. After two months, the samples were taken out for Scanning Electron Microscopy (SEM) analysis. The particle population found from the SEM sample grid was categorized to a particle size number distribution and the morphology of the particles was shown.

Particle viscosity can be investigated indirectly by measuring the diffusion rates for certain molecules through SOA particles and by assuming Stokes-Einstein to be valid. Indirect measurements can be divided into diffusion measurements (Abramson et al. 2013), evaporation measurements (Cappa and Wilson 2011, Vaden et al. 2011) or reactivity studies (Kuwata and Martin 2012, Perraud et al. 2012, Zhang et al. 2015). Abramson et al. (2013) reported viscosity values for SOA particles by measuring a mixing of pyrene molecules and clusters through the SOA particles. Perraud et al. (2012) studied the diffusion of nitrates in SOA particles phase whereas Cappa and Wilson (2011) reported the diffusion coefficients for α-pinene SOA particles based on their chemical composition after a heating process. In addition, Lienhard et al. 2014, Lienhard et al. 2015, and Price et al. (2014) focused more on reporting water diffusion coefficients for α-pinene SOA rather than on showing viscosity values. Lienhard et al. (2014) used an Electric Dynamic Balance (EDB) system to study levitated water-solvent SOA material while measurements in Price et al. (2014) and Zobrist et al. (2011) were based on Raman spectroscopy. Bateman et al. (2015) reported viscosity values for common biogenic laboratory SOA particles according to their bounce measurement results for sucrose.

Despite the various combinations of direct and indirect phase state measurement methods, the method based on the measurements of particles' mechanical bounce is currently the only method available for capturing real-time ambient SOA observations. Virtanen et al. 2010, Bateman et al. 2016, and **Paper III** have estimated the phase state of SOA particles based on real ambient field measurements. Virtanen et al. (2010) found that major fraction of atmospheric submicron aerosol particles were amorphous solids in the boreal forest environment in Hyytiälä, Finland. Bateman et al. 2016 and **Paper III** found atmospheric SOA particles staying primarily liquid in ambient conditions in Amazonia and the Southeastern US, respectively. None of the current methods has been able to draw an accurate estimation between the viscosity of the ambient SOA particles, T and RH, but all of them have found SOA particles to be composed of amorphous material, meaning RH-dependent viscosity.

3.1.1 Aerosol bounce instrument (ABI)

The first steps in aerosol bounce studies were taken by Virtanen et al. (2010) who found ambient SOA particles existing in a solid/semisolid phase state by studying their behavior in an electrical low pressure impactor (ELPI, Dekati ltd). A multi-stage particle impactor did not capture all of the particles

due to the bounciness of particles inside the impactor system. Before that, biogenic SOA particles were generally assumed to be in liquid form (Seinfeld and Pandis, 2006). Based on the ideas shown in Virtanen et al. (2010), a new method was introduced in Saukko et al. (2012a), and further used in Saukko et al. (2012b), and Saukko et al. (2015). Due to forthcoming scientific questions, a further improved version (i.e., broader RH range, broader particle size range, pressures closer to ambient conditions) of the bounce system was built and used in **Papers II** and **III**. The revised version of the bounce system was named the Aerosol Bounce Instrument (ABI). However, at the same time, Bateman et al. (2014) also introduced their own "rebound apparatus", which was later used in Bateman et al. (2015), Bateman et al. (2016) and Li et al. (2015).

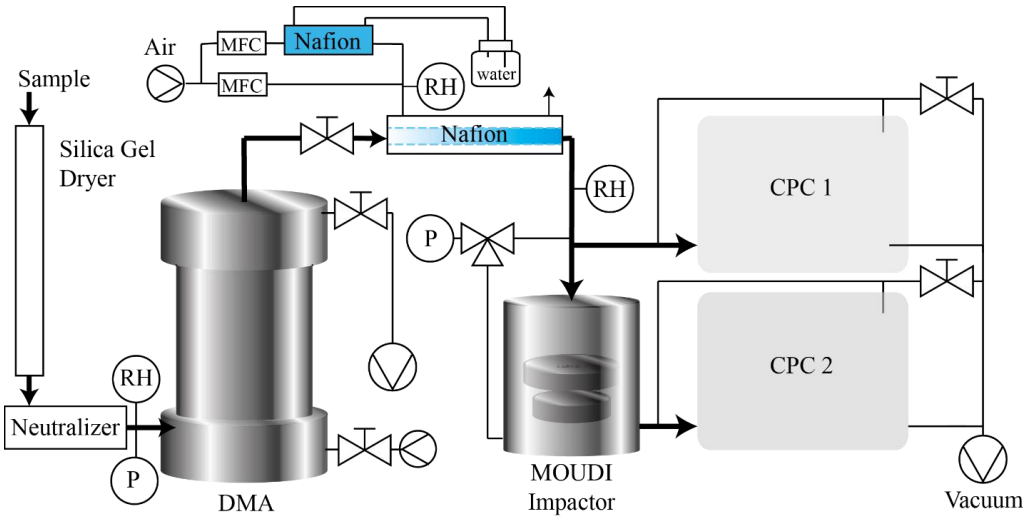

Figure 3.1. | Aerosol Bounce Instrument (ABI). Schematic representation of the measurement set-up used in the bounce experiments. The thick line represents the sampling line, CPC 1 and 2 are condensation particle counters (TSI, 3010), P denotes the pressure gauge, DMA is a differential mobility analyzer and RH denotes a humidity sensor (Vaisala, HMP110). The figure is adapted from **Paper II** and the Supplementary therein.

The ABI consists of an aerosol size selection unit, humidifier unit, impactor apparatus, and two particle number counters. The schematics of the ABI is shown in Fig. 3.1. At first, the particles are dried prior to the measurements by passing the sample air through a Silica-gel diffusion drier. The estimated time for the particles spent in the dried zone is typically around 5 seconds. After that, the size-selected particle population of the particles is classified with a Differential Mobility Analyzer (DMA; Knutson and Whitby, 1975). In **Papers II** and **III,** a custom-made, medium length (l=0.11m, r_1=0.025m, r_2=0.033), Vienna-type DMA was used in the ABI leading to a residence time of around 0.8 – 0.9 seconds inside the DMA. The monodisperse particle population is then passed through a Nafion multitube humidifier (Permapure®, PD-110-50). RH is controlled by mixing dry and saturated air on

the outer flow of the Nafion tube. This is done by digitally PID-controlling the flows with two mass flow controllers (MFC, see Fig. 3.1) and using fixed RH as a PID-setpoint. The residence time of the aerosol in the humidified region before the particles enter the impactor is approx. eight seconds. RH is measured with a RH probe (Vaisala HMP110) just before the MOUDI single stage impactor, where the actual bounce process takes the place. Seventy etched microscopic holes are left open in the MOUDI orifice plate (originally 2000 etched holes), and pressures prior to and after the impactor are controlled manually with needle valves, and with an extra vacuum line in the bypass flow of the impactor. Finally, particle number concentration is measured both at the in- and outlet of the impactor, with two separate condensation particle counters (CPC, TSI, model 3010). CPCs are modified such a way that they are capable to operate at a slightly lower pressure than ambient (600 – 1000mbar). In practice, the butanol saturator column was connected to the same air stream as the outer flow of the impactor (equaling the pressure in the saturator and CPC inlet), and an extra exhaust filter of the CPC was ejected and the pipe was plugged.

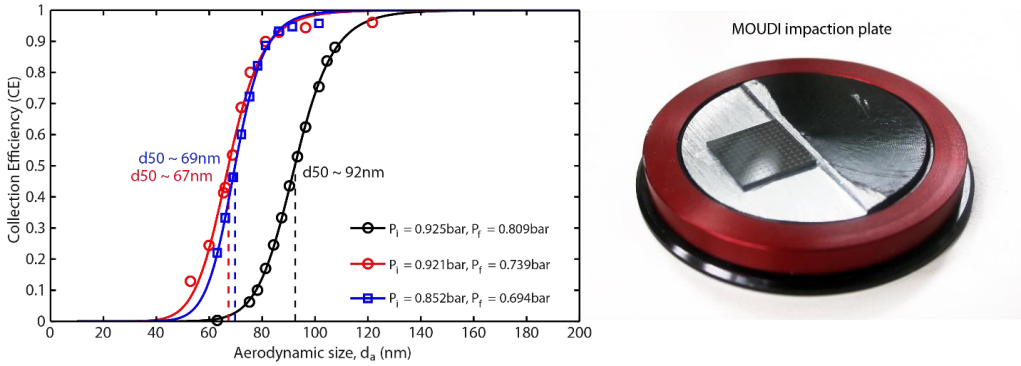

Figure 3.2. | Calibration of single stage MOUDI impactor. On the left: collection efficiency (CE) measurements and sigmoid fits to the experimental data points. The performed pressure conditions for each calibration curve are listed in the legends (initial and final pressures). On the right: A picture of the modified MOUDI impactor plate. The black half of the plate is the original MOUDI plate and the polished one is modified for grid sampling (the grid attached to the plate in the picture).

The MOUDI single stage impactor needs to be calibrated to operation pressures. This was done by measuring the collection efficiency (CE) of the impactor stage with completely liquid dioctyl sebacate (DOS) oil particles. DOS particles were generated by steaming liquid DOS in a flow-through oven and letting it nucleate in supersaturated conditions by cooling down the flow stream right after the oven. The actual CE measurements were done in a similar fashion to the typical bounce measurements introduced above, and with the same impactor plate. The cut-off size of the impactor plate (d_{50}) is defined as an aerodynamic diameter of a particle for which the CE is 50%. d_{50} was derived by fitting an empirical $C_E(d_a)$-sigmoid function to the measured DOS data. The CE-curve can be written as (Saukko et al. 2012)

$$C_{\mathrm{E}}(d_{\mathrm{a}}) = \frac{1}{1+\left(\frac{d_{50}}{d_{\mathrm{a}}}\right)^{2\delta}} \quad (22)$$

where the aerodynamic diameter of the particles, d_a, can be calculated with the equation (Hinds 2012)

$$d_a = d_p \left(\frac{C_C(d_p)}{C_C(d_a)}\right)^{1/2} \left(\frac{\rho_e}{\rho_0}\right)^{1/2} \quad (23)$$

where C_C is the Cunningham slip correction factor, ρ_e and ρ_0 are the effective densities of the particle matter and water, respectively, and d_p is the mobility diameter (selected with the DMA). The resulted calibration curves are shown in Fig. 3.2.

Table 3.1. | Impactor calibration variables. The parameters of the sigmoidal CE curves (d_{50} and δ) used in equation (22) for calibration of MOUDI single stage impactor plate are listed below. In addition, the specified impactor inlet and outlet pressures, P_i and P_f, are listed. In **Paper I** and **II**, the pressures listed in the first row in the table were used in the measurements.

P_i (mbar)	P_f (mbar)	d_{50} (nm)	δ
850	700	69	6.674
925	800	92	5.956
920	740	67	6.292
750	600	56	5.525

The final bounced fraction can be calculated as

$$\mathrm{BF} = \frac{B' - (1 - C_E(d_a))}{B_{\mathrm{ref}} C_E(d_a)}, \quad (24)$$

where $C_E(d_a)$ is the collection efficiency at the aerodynamic size d_a, and B' is the uncorrected (measured) ratio between the CPC readings. The reference fraction, B_{ref}, is measured with the impactor, but without an impactor plate installed to characterize the relative ratio between two CPCs and the particle losses to other deposition surfaces than the impactor plate. B_{ref} was measured on daily basis before and after the data collection. It was also measured in different RH, and using different particle composition and different particle size, to characterize the possible effects of the particle properties on it. The dependency of the B_{ref} on RH and particle composition was negligible. Particle size had an effect on B_{ref} but within the size range used in this thesis, the effect was negligible. Selected particle sizes used in all measurements of this thesis were chosen to be big enough to have a collection efficiency approx. unity. Particle concentration in the sample air was always low enough (< 200 cm^{-3}) to ensure that the particle loadings on the impactor plate were negligible. The effect of loading on the

bounce was also studied. The loading of liquid particles such as deliquesced ammonium sulphate particles clearly decreased the actual BF, but after drying the impactor low enough (i.e., below ERH of AS), the BF values recovered to the initial level. To minimize the effect of loading on the BF, the aluminium foil on the plate was replaced frequently. Moreover, RH was kept below 95% during the measurements to avoid the condensation of saturated water on the walls and on the impactor plate. Investigated laboratory single-component solutions are listed in table 3.2, with ABI measurement ranges for each compound.

Table 3.2. | Laboratory substances tested with the ABI. During the ABI evaluation and the measurement campaigns, the ABI was systematically tested with the solutions listed below. Molecular weight (M_w) of the compounds as well as measurement ranges of particle dry diameter (d_a, aerodynamic), temperature and RH (impactor upstream) are listed. The silicone particles were nebulized from n-heptadecane solution. Other compounds were nebulized from a water solution with a TSI atomizer.

Solute	M_w (g/mol)	d_a (nm)	T (°C)	RH (%)
Ammonium sulfate	132	80 - 300	-15 - 25	0 - 90
Sucrose	342	80 - 300	7 - 25	0 - 90
Glucose	180	80 - 300	7 - 25	0 - 90
Trehalose	342	120 - 220	20 - 25	0 - 90
Citric acid	192	120 - 220	20 - 25	0 - 90
Methylglyoxal	72	120 - 220	25	0 - 90
Silica	60	80 - 160	25	0 - 90
Silicone (100 - 20000 Pas)	n/a	120 - 150	25	0 - 75
Dioctyl sebacate (DOS)	427	10 - 300	25	0 - 50
Bovine Serum Albumin	>65000	80 - 300	25	0 - 90
PSL, Latex beads	n/a	100, 300	25	0 - 90

3.2 Hygroscopicity, growth and shrinking measurements

Hygroscopicity denotes the capability of particles to uptake water vapor. Thus, it is an application of a general gas-partitioning process (Seinfeld and Pandis, 2006). In this thesis, the volatility and hygroscopicity of SOA particles were studied by measuring particles' change in size after a desired treatment by a Tandem Differential Mobility Analyzer (TDMA; Rader et al. 1986) system. In the hygroscopicity measurements, particles were humidified at fixed RH and the consequent increase in particle size was measured (**Papers II**, **III**). In the volatility studies, the desired treatment was the

dilution of the gas phase in an evaporation chamber, allowing the variation of the residence time (**Paper IV**). A similar approach was recently used in a volatility study in Vaden et al. (2011). Other SOA volatility studies have been mainly based on thermodenuder experiments (e.g., Tritscher et al. 2011, Häkkinen et al. 2012, Hong et al. 2014, Cerully et al. 2015) and the latest studies have combined residence time variation and denuder treatment (Karnezi et al. 2014; Saha et al. 2015; Saha et al. 2016).

The water uptake of aerosol particles can take place in sub- or supersaturated conditions. Also current hygroscopicity measurement methods are categorized to these saturation ranges. The hygroscopicity of aerosol particles can be measured with multiple methods. Defining particle-phase liquid water content by comparing DMPS distributions of dried and humidified (RH<100%) samples (Nguyen et al. 2014) is applicable at very low concentrations, but the resolution of the method is not as high as in measurements done using monodispersed aerosol. Moreover, light-scattering methods have been widely used since they have a direct relationship to the climate relevance (Attwood et al. 2014, Brock et al. 2016, Rosati et al. 2015). In this thesis, the hygroscopicity of monodispersed SOA particles is studied by measuring the change in size between dry and fixed RH with Hygroscopic-TDMA (HTDMA; Liu et al. 1978), which is an accurate method to study the water uptake of submicron aerosol particles at subsaturation conditions (Petters and Kreidenweis, 2007). Supersaturation measurements for SOA particles were conducted by studying their CCN activation with a Cloud Condensation Nuclei counter (CCNc; Roberts and Nenes, 2005) at supersaturated conditions.

3.2.1 TDMA systems to measure growth or evaporation

Particle size evolution is a crucial scientific topic to investigate. Condensational growth by water, other atmospheric trace gases, or relevant organic vapors can be measured simply by defining the initial size of the particles and measuring their size after the desired treatment. In the treatment section, the particles are pushed out of the thermodynamic equilibrium, which triggers the mass exchange between gas and condensed phase. The particles can be pushed out of the equilibrium in various ways, for example by changing temperature, cleaning the surrounding gas-phase, by adding moisture or other condensable vapor to the gas-phase, or by exposing aerosols (or vapors) to UV radiation. The characterization in size upstream and downstream of the treatment remains the same but the treatment is varied according to the scientific question. This principal was already conducted in Twomey, 1971. Intuitively, the simplest way to study the evaporation and volatility of the SOA compounds would be by heating the particles between the two DMAs (Orsini et al. 1999). This has been the traditional way to investigate the volatility of SOM (Tritscher et al. 2011). However, by heating we would introduce uncertainties to the characteristic enthalpy of vaporization. This is why in this thesis, all the measurements were done at around room *T,* and the evaporation was created by diluting the gas-phase (**Paper IV**).

The general schematics of the TDMA approach are illustrated in Fig. 3.3. In general, the dried polydisperse particle population (green curve in Fig. 3.3) is charged with a neutralizer prior to the first DMA (DMA1). Then, the lognormal monodisperse particle population (red curve in Fig. 3.3.) is selected with DMA1 and is passed through the desired treatment section. The resulting size distribution of the particle population (brown or blue curve in Fig. 3.3.) exposed to the desired conditions is then

measured by scanning the voltage controlling the second DMA (DMA2) and continuously logging the number concentration of particles passed through the DMA2 with a CPC.

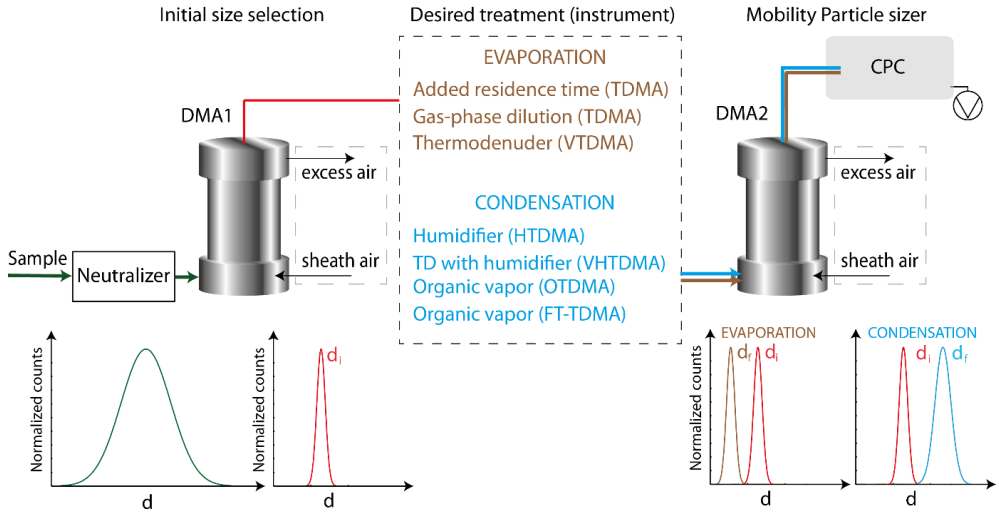

Figure 3.3. | TDMA systems. The schematics of the TDMA set-ups used in evaporation/condensation or hygroscopicity measurements. The optional treatments are listed in the dashed box in the middle. The green normal distribution curve represents the initial polydisperse aerosol sample, the red curve illustrates the monodisperse particle population selected with the first DMA (DMA1), and the brown and blue bell curves represent the final size distribution measured with the mobility particle sizer consisting of the second DMA (DMA2) and a CPC. The brown curve illustrates the measured size distribution of the evaporated particles (i.e., $d_i > d_f$), whereas the blue curve represents the size distribution of grown particles ($d_i < d_f$).

The desired treatments in the TDMA systems can be divided into evaporational and condensational methods (see Fig. 3.3.). For instance, Saha et al. (2016) investigated the volatility of ambient SOA particles by varying both residence time and thermodenuder temperature during the SOAS campaign. Cerully et al. (2015) studied SOA volatility during the SOAS campaign by varying the temperature in thermodenuder. The evaporation is usually reported as a ratio between the resulting size, d_f, and initial size, d_i, or a ratio of their surface areas/volumes (Vaden et al. 2011).

The TDMA approach with a dilution and adjustable residence time was conducted in an evaporation study in **Paper IV**. In that case, the carrier gas of the particles was diluted in the DMA1. The method relies on laminar flows inside the DMA1. Hence, the gas phase mixing of sample flow and sheath air flow should take place only due to the diffusion of the gas molecules., The size-selected aerosol is stored after dilution in a clean (both gas and particle phase) polished stainless steel chamber reactor, where particles evaporate towards equilibrium based on their volatility. The setup used in **Paper IV** is shown in Fig. 3.4. and described below in more detail.

In the measurements reported in **Paper IV**, the SOA particles were generated with a flow tube (FT) from ozonolysis of α-pinene at dry conditions (RH<30%). The size selection and dilution were done simultaneously in the DMA1. By using clean air in the DMA1 sheath flow and by using nano-DMA (TSI), having a very short tube length and hence, very short residence time inside the DMA1, we were able to minimize the mixing caused by gas-phase diffusion. The vapor wall loss rates inside the residence time chamber (RTC) were assumed to be fast (see details in SI of the **Paper IV**). Based on our measurements, very high dilution ratios (higher than 1:100) were achieved by the set-up. Moreover, potassium iodide coated copper tubing was added to the downstream of FT to scavenge high ozone concentration before the DMA1. The size-selected particles were pulled to a residence time chamber (RTC) for a desired time. In **Paper IV**, the evaporation process took place in a clean stainless steel RTC at three different RHs: RH < 5% (dry), RH ~40% and RH ~80%. This was done by humidifying the sheath air of the DMA1. The TDMA system was size-calibrated (and RH-calibrated) by measuring multiple dry (and wet) sizes for atomized ammonium sulfate particles. Residence times between 2 seconds and 350 minutes were studied, and the ratio between the final and the initial size (d_t / $d_{t=0}$) of the particles was reported. The selected initial size was 80 nm.

The hygroscopicity of the particles was studied using HTDMA (**Paper II** and **III**). HTDMA is the most powerful tool to measure the water uptake of submicron aerosol particles in subsaturated conditions (RH < 100%) and the basic operational principle was introduced by Liu et al. (1978). In practice, HTDMA measures hygroscopic growth factor (GF) which equals wet diameter ($d_f = d_{wet}$) divided by the particles' initial dry diameter ($d_i = d_{dry}$). In traditional HTDMA systems, RH is set to fixed 90% RH (Gysel et al. 2007) and multiple dry sizes can be measured, but recent studies have also investigated water uptake at varied RH (e.g., Mikhailov et al. 2009, Wex et al. 2009, **Paper II**). In **Papers II** and **III**, the closed loop DMA configuration was used to prevent the evaporation of semi volatiles from the particles inside the DMAs.

Usually, hygroscopicity κ derived from HTDMA measurements is calculated with eq(8), and by replacing the particle wet size by GF and dry size, d_{dry}, as

$$\kappa_{HGF} = 1 - GF^3 - \frac{(GF^3-1)}{RH} e^{\frac{4\sigma_S M_W}{RT\rho_W d_{dry} GF}} \quad (25)$$

where d_{dry} is particle size selected with the DMA1, RH is the fixed RH in the DMA2, ρ_w is the density of water, σ_s is the surface tension of SOA particles (here assumed surface tension of water at room T, 0.072 N m^{-1}), M_w is the molecular weight of water, T is temperature and R is the universal gas constant. In **Paper II**, the SOA particles were considered as pure organics. In a case where the particles are composed of inorganic and organic components (**Paper III**), the hygroscopicity of the organic fraction (κ_{OA}) can be estimated from the total hygroscopicity (κ_{tot}) measured by the HTDMA using κ-mixing rule (Petters and Kreidenweis 2007). In general, the hygroscopicity of multicomponent aerosol particles can be calculated as a sum of the contributions of each component (Petters and Kreidenweis 2007). Thus, the mixing rule (eq(14)) can be separated into the organic (OA) and inorganic (inorg) fractions as (eq(15)):

$$\kappa_{tot} = \sum_{i=1}^{n} f_i \kappa_i \quad (26)$$

$$= f_{\mathrm{OA}}\kappa_{\mathrm{OA}} + f_{\mathrm{inorg}}\kappa_{\mathrm{inorg}} \quad (27)$$

where f_i and κ_i are the volume fraction and hygroscopicity parameter of component i, respectively (Petters and Kreidenweis 2007). The volume fractions of organic and inorganic species, i.e., ammonium sulfate (AS), ammonium bisulfate (ABS), sulfuric acid (SA) and ammonium nitrate (AN), are derived from AMS mass fractions using the literature densities listed in **Paper III**. The hygroscopicities of many inorganic species can be calculated with the E-AIM model (Clegg et al. 1998), and are well-reported elsewhere. Our approach assumes also that organics are mixed into one phase and that their average hygroscopicity can be described with single κ_{OA}. Instead, Cerully et al. (2015) reported isolated κ values for OA fractions of different volatilities, i.e., $\kappa_{\mathrm{LV\text{-}OOA}}$, $\kappa_{\mathrm{SV\text{-}OOA}}$.

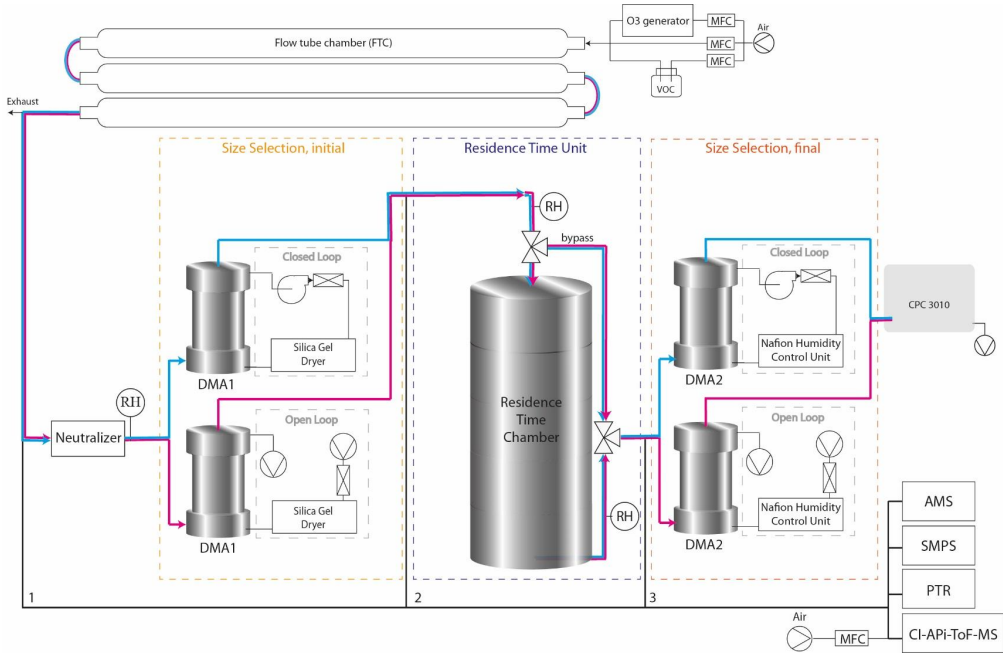

Figure 3.4. | Set-up for the evaporation study. Schematic representation of the TDMA setup used in the evaporation experiments (**Paper IV**). The pink thick line represents the sample line used in the open loop DMA configuration, whereas the blue line represents the sample line in the measurements where closed loop DMAs were chosen. The particle size and gas-phase conditions were measured prior to and after the RTC treatment.

If the particles are initially spherical, the change in size is easy to measure accurately. This is a common general assumption, and also many times, a valid one. However, in some cases the particles' morphology is non-spherical, which has to be taken into account with a shape factor (χ) when estimating the actual size of the particles (Hinds, 2012). In this thesis, the particles were always assumed to be spherical (i.e., χ = 1). Typical residence time in the humidified region in HTDMA systems varies between 1 – 15 seconds. By adding an extra residence time chamber to the system

between the DMAs, the average residence time can be extended up to a number of hours. The residence time in the treatment section was approximately eight seconds in the studies of **Papers II** and **III,** whereas in the evaporation experiments reported in **Paper IV** the time scale in evaporation chamber was from 1 second up to three hours.

3.2.2 CCNc to measure cloud activation

The activation of submicron aerosol particles to form cloud droplets is determined by the particle size, composition and water vapor supersaturation (McFiggans et al. 2006). A Cloud Condensation Nuclei counter (CCNc) is built to simulate cloud activation process in a short time and small space, and in such a way that the activation can be measured on-line continuously (Roberts and Nenes 2005). Continuous-flow thermal-gradient CCN counter from Droplet Measurement Technologies (DMT-CCNc) was used in this thesis (**Paper II**). In CCNc setup, the dry particles are passed through a neutralizer and a DMA, and the initial particle number concentration of the size-selected population is measured with a CPC. Then the particles are exposed to the effective water vapor supersaturation, SS%, in a *T*-controlled column and the formed droplets are optically countered with an optical particle counter (OPC). Typically, the selected dry particle size, d_p, is kept constant and T in the column is varied so that the activation spectra scans from 0% (no activation) to 100% (all particles activated).

At each critical dry size, d_c, the corresponding critical super-saturation, S_c, can be calculated from the standard Köhler-theory, assuming the surface tension of pure water and complete dissociation of ammonium sulfate (AS) in the solution (in the calibration phase). In practice, S_c is derived from the CCNc measurements by fitting sigmoidal function to the activation data and deriving supersaturation where the fitted curve equals 50% activation. The CCN hygroscopicity parameter, κ_{CCN}, can be calculated using CCN data with equations given by

$$\kappa_{CCN} = \frac{4A_{Kelvin}{}^3}{27 d_c{}^3 \ln^2 S_c}\ ,\ A_{Kelvin} = \frac{4\sigma_w M_w}{RT\rho_w}, \qquad (28)$$

where A_{Kelvin} is the same Kelvin-term used in eq(7), σ_w is the surface tension of water, M_w is the molecular weight of water, R is the gas constant, T is temperature and ρ_w is density of water. Recently, *κ-Köhler theory* has been modified to take into account insoluble parts at supersaturation (Kumar et al. 2011). In this thesis, however, all the studied SOA particles were assumed to be fully soluble at supersaturation conditions and thus the eq(15) was applied for all compounds.

3.3 Laboratory and field measurements

Ambient measurements are often replicated in laboratory conditions to study the specific processes and properties of SOA particles, and also to quantify the representative factors for climate models. The particle formation and growth mechanisms remain similar, but both particle and gas-phase concentrations are typically higher than in the atmosphere. In this thesis, the laboratory aerosols were generated from gaseous precursors with either a continuous flow Potential Aerosol Mass (PAM) reactor (**Paper II**), Teflon chamber (**Paper I**), an oxidation flow reactor (OFR; **Paper III**), or a

continuous flow tube (FT) reactor (**Paper IV**). Other laboratory test substances such as Silica, PSL, AS and BSA were generated from a water solution with a constant output aerosol nebulizer.

Particle composition. Aerosol Mass Spectrometry is the most widely used method to resolve both particle composition and size online (Jayne et al. 2000). In this thesis, non-refractory submicron (PM_1) particle-phase mass distribution was monitored by an Aerodyne High Resolution Time-of-Flight Aerosol Mass Spectrometer (HR-ToF-AMS, hereafter called AMS). In laboratory measurements (**Paper II, IV**), it was used to quantify the elemental composition (oxygen to carbon ratio, O:C and hydrogen to carbon ratio, H:C) for organics, while in ambient studies (**Paper II, III**), the fraction of organics and inorganic species were estimated in addition.

3.3.1 SOA generation in a laboratory

The precursors of SOA particles, VOCs, are defined based on their initial molecular form. Isoprene is the smallest terpene, a chainlike molecule consisting of five carbon atoms with two double bondings between the carbon atoms. Correspondingly, monoterpenes consist of two isoprene units with 10 carbon atoms and sesquiterpenes contain 15 carbon atoms, and both have from one to several double bondings. As the precursor molecules transform via reactions with OH radicals, ozone, NO_3, and photochemistry, a complex variety of the oxidation products of the precursors are formed, leading to various molecular structures and functional groups. The higher the precursor carbon number, the greater number of different oxidation products are formed (Kroll and Seinfeld, 2008). In oligomerization, carbon chains are attached together forming even longer molecules (typically, no change in O:C). Fragmentation instead denotes the process where the carbon chain is cut and two smaller molecules are formed. In functionalization, an oxygenated group is added to the original carbon chain (thus, O:C is increased). All the changes in molecular structures have an effect on the physical properties of the compounds, such as volatility (Donahue et al. 2011), solubility (Riipinen et al. 2011) and hygroscopicity (Jimenez et al. 2009). Generally, oligomerization and functionalization decrease the vapor pressure of the compound. Fragmentation instead sometimes creates higher vapor pressure compounds and sometimes the vapor pressure is reduced because the formed species are also functionalized. A common example is the ozonolysis reaction of monoterpenes. While the double bond is broken, at least two oxygen atoms are added, often clearly decreasing the vapor pressure of the products compared to the parent-molecule. In this work, SOA particles were generated by oxidizing the precursor VOCs in the laboratory in a controlled environment. The utilized SOA generation systems are briefly described in the following paragraphs.

PAM reactor. In **Paper II,** the studied SOA particles were generated from single precursor at a time, using either α-pinene- ($C_{10}H_{16}$), isoprene- (C_5H_8) or longifolene- ($C_{15}H_{24}$) as a precursor VOC gas. The precursor gas was injected to the 30l glassy PAM reactor (Lambe et al. 2011) with N_2 as carrier gas. Total flow through the PAM was kept constant at 8.5lpm and the RH was kept around 30%. Inner UV lamps were used to generate OH from water and O_3 by photochemistry. The OH concentration in the reactor was controlled by adjusting the intensity of the UV lamps. With very high OH exposure, a higher oxidation state (higher O:C) of the particles was achieved. The OH

concentration was varied for α-pinene and longifolene, resulting in an O:C range of 0.39 - 0.7 for the generated SOA, while the isoprene SOA was produced with only one UV exposure.

In **Paper IV**, the studied SOA particles were produced by ozonolysis of α-pinene using the self-made glass flow tube which is schematically described in Fig. 3.5. Purified air was used as a carrier gas for ozone, and VOCs. α-pinene was added to the air stream from a small vessel (0.1lpm flow through it). SOA particles formed in a flow tube by ozonolysis and the outflow was monitored with the AMS and a scanning mobility particle sizer (SMPS, TSI), while the gas-phase compounds were measured with a proton-transfer-reaction time-of-flight mass spectrometer (PTR-ToF-MS, Ionicon), and a chemical ionization ambient pressure interface time-of-flight mass spectrometer (CI-APi-ToF-MS, Tofwerk).

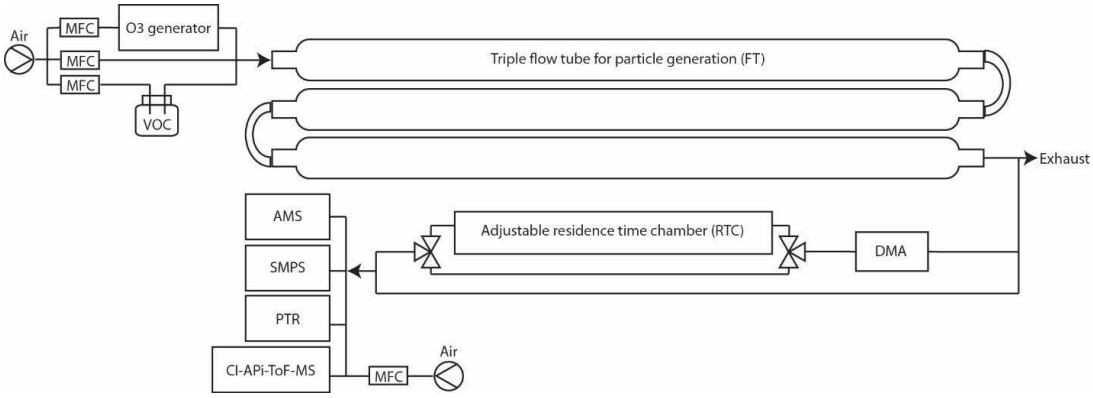

Figure 3.5. | Continuous flow tube SOA generation system. Schematic representation of the SOA generation set-up used in the evaporation experiments (**Paper IV**). The initial gases provide the production of OH radicals for the oxidation of the SOA precursor (VOC bottle).

3.3.2 Field measurements

In this thesis, **Paper II** and **Paper III** comprise data from field measurements. Comparison data from ambient observations for laboratory SOA analysis in **Paper II** were collected at SMEAR II station (Hari and Kulmala, 2005) in central Finland, Hyytiälä (61^{o} 51'N, 24^{o} 17'E), between May 9th and June 3rd, 2013. The station is located in remote boreal forest (mainly Scots pine trees), and the closest populated city (Tampere) lies approx. 60 kilometers away from the measurement station. In Hyytiälä monoterpene emissions have been shown to comprise the vast majority of the atmospheric aerosol (Finessi et al. 2012; Raatikainen et al. 2010). HTDMA measurements were performed at fixed RH=90% for 100 nm dry particles (Hong et al. 2014), the CCNc column was saturated to 0.2 and 0.3 %SS (Paramonov et al. 2013), and HR-ToF-AMS measurements were utilized for submicron PM composition. The dry particle size distribution was monitored with the Differential Mobility Particle Sizer (DMPS).

The field measurements reported in **Paper III** were conducted in Southeastern US, Alabama (61^{o} 51'N, 24^{o} 17'E), from June 1^{st} to July 15^{th}, 2013. The Southeastern Aerosol and Oxidant Study (SOAS) campaign gathered over 150 aerosol scientists together to study atmospheric processes using a comprehensive set of measurement devices for the chemical and physical characterization of vapors and aerosols. HTDMA, AMS, DMPS, and ABI set-ups were utilized in the campaign and used in the analysis in **Paper III**. In addition, meteorological data were available in the measurement site.

OFR reactor. In addition to the ambient measurements, OFR was used during the SOAS campaign to investigate OA formation (and aging) from ambient air. The operation principle of the OFR is similar to the operation principle of the PAM described above. The studied ambient particles were injected to the OFR straight from the ambient. RH and T were allowed to vary inside the OFR depending on the ambient conditions, and UV was varied in five 10min steps leading to the initiation of photochemistry and thus, a wide range of OH exposures (10^{10} – 10^{13} molec. cm^{-3} s) compared to the ambient natural OH variation. Total flow through the OFR was kept constant at 3.5 – 4.2lpm resulting in a gas-phase residence time of approx. 200 seconds. ABI and AMS were measured alternatively ambient and through OFR, whereas HTDMA measured ambient air only. The particle number size distribution was also monitored in both from ambient and through the OFR with DMPS.

4. Results and discussion

In this chapter, the results with the interpretations from the SOA experiments are discussed. Estimated viscosity ranges for α-pinene ozonolysis SOA particles and real pine-VOC ozonolysis SOA at dry conditions are studied in **Paper I**. The water uptake of semisolid SOA particles and the factors controlling it are investigated in **Paper II**. In **Paper III,** the particle bounce measurements were performed in atmospheric conditions to study the linkage of the particle phase, oxidation state, and hygroscopicity in rural ambient conditions in Alabama, US. In addition, the enhanced oxidation (i.e., O:C) of ambient aerosol particles in the OFR and proposed changes in their physical properties are discussed. The evaporation kinetics of α-pinene ozonolysis SOA in different RH conditions are studied in **Paper IV**.

4.1 Laboratory SOA particles

4.1.1 Viscosity range of SOA particles at dry conditions

SOA particles' coalescence, i.e., structural changes from agglomerates into the spherical form, was studied in **Paper I** to infer the viscosity of the particles. Oxidation products from the ozonolysis of real pine-VOCs nucleated in the presence of SO_2 to form SOA particles in a laboratory environment, namely a Teflon chamber. The particles were collected onto SEM filters and stored at relatively dry conditions (RH < 30%) for approximately two months. As can be seen from Fig. 4.1., the SEM images reveal the existence of agglomerates on the collection substrates. The viscosity range of the SOA particles can be estimated with the eq(4) if their shape change from agglomerate into spherical form is detected. As can be seen in Fig. 4.1., the collected pine-SOA particles still remained as non-spherical

agglomerates after two months, indicating that the coalescence time-scales are longer than the storage time. By using eq(4), we can estimate the lower limit for the viscosity of the pine-SOA particles to be greater than 10^{12} Pa s. Similar SOA generation was conducted for α-pinene without the presence of SO_2. The initial particle concentration was comparable to the pine-SOA experiments and the sample collection time remained the same in both experiments. Thus, the coagulation rates of the primary particles observed in images b and c (Fig. 4.1.) can be assumed to be of similar magnitude. However, the α-pinene SOA particles were coalesced to a fully spherical form. In other words, the viscosity of the α-pinene SOA particles was low enough ($\eta < 10^{12}$ Pa s, according to eq(4)) for the coalescence to occur within the storage timescale (two months).

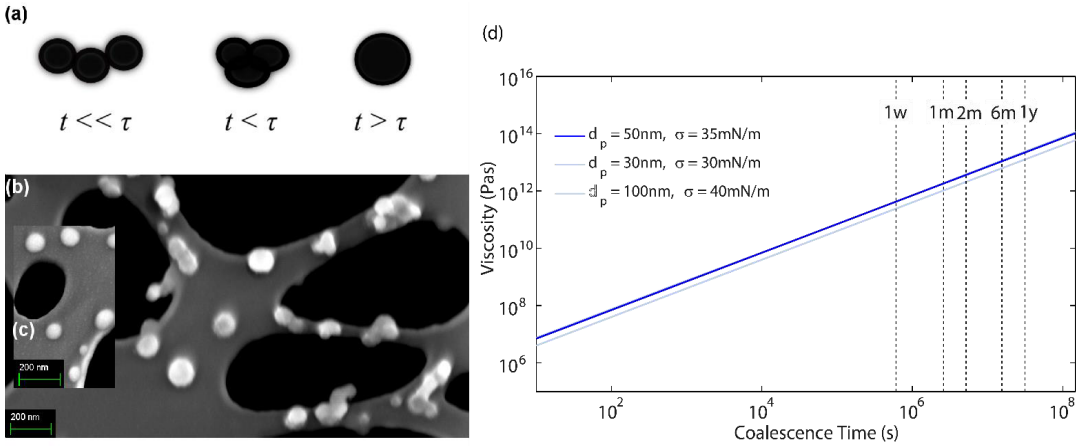

Figure 4.1. | Estimated coalescence time for SOA particles. In a) a schematic presentation of the coalescence process, b) a SEM picture of pine-SOA particles, c) a SEM picture of α-pinene SOA particles, and in d) a viscosity range with coalescence time for different particle sizes (30 – 100 nm) and particle surface tensions (30 – 40 mN m^{-1}).

These results indicate that the pine-SOA particles are glassy solid at dry conditions in room *T*, while α-pinene SOA particles are in a semisolid phase. These results are in line with the results of other recent phase state studies (Abramson et al. 2013, Cappa and Wilson 2011, Kuwata and Martin 2012b, Renbaum-Wolff et al. 2013, Saukko et al. 2012, Virtanen et al. 2011, Virtanen et al. 2010, Zhang et al. 2015). The coalescence time approach has recently also been applied in other studies to quantify the viscosity of SOA particles. Zhang et al. (2015) used the same approach to estimate viscosities at *T*=293K for α-pinene particles and determined the viscosities at RH<5% and RH=58% to be $10^{(8.7\pm2)}$ Pa s and $10^{(7.0\pm2)}$ Pa s, respectively. In addition, Järvinen et al. (2016) used a similar approach and investigated structural change from agglomerate to spherical form of α-pinene SOA particles at low temperatures (-10°C - -38°C). They estimated the viscosity of 400 nm sized primary α-pinene particles to be in the order of 10^7 Pa s.

4.1.2 Phase transition RH of SOA particles with varied composition

In **Paper II**, we show the phase transition curve for α-pinene- ($C_{10}H_{16}$), isoprene- (C_5H_8) and longifolene- ($C_{15}H_{24}$) SOA with a varied degree of oxidation (O:C) based on ABI measurements. The BF curves are shown in Fig. 4.2b. α-pinene SOA particles produced by ozonolysis in a PAM chamber turn liquid (i.e., the BF reached zero, $RH_{BF=0}$) at ~88%RH. When SOA particles were produced with photochemistry, leading to clearly higher O:Cs, the phase transition RH decreases as low as 75% RH for α-pinene SOA with O:C ~0.7. A similar trend between O:C and phase transition RH is shown for longifolene-derived SOA; as O:C is changed from 0.39 (ozonolysis) to 0.83, $RH_{BF=0}$ decreases from >95% to ~82%. Isoprene-derived SOA particles (O:C = 0.86) transform to liquid at RH~62%. These results indicate that that not only does O:C correlate with phase transition RH, but also the molecular weight of the precursor vapor has an impact on the physical phase state of resulting SOA particles. All of the measurements related to **Paper II** were done at room *T*. Despite these findings the ABI measurements were not sensitive enough to capture the effect of O:C on the viscosity of the dry particles. All the ABI humidograms level off at RH < 30% and no significant differences between the different SOA types were seen. The BF results at dry conditions are in good agreement with previous bounce studies (Saukko et al. 2012, Bateman et al. 2015).

Most of the recent RH-induced phase transition studies for SOA particles are compared in Li et al. 2015. Bateman et al. (2015) estimated that α-pinene-SOA transformed into liquid when RH exceeded 70%. A similar transition RH was reported by Renbaum-Wolff et al. (2013). Kidd et al. (2014) instead concluded that phase transition from solid to liquid occurs at RH~80% for α-pinene-SOA at room temperature. A similar RH range for α-pinene was drawn by Song et al. 2015. Zhang et al. (2015) reported α-pinene SOA to be composed of semisolid (η ~10^7 Pa s) material even at RH=58%. By contrast, Denjean et al. (2015) speculated that α-pinene SOA experiences phase transition already at RH~35%. These differences in reported RH-induced phase transitions for α-pinene-SOA highlight the influence of the utilized measurement method, studied particle size range, and measurement set-up on the final estimations. Particular care is needed in listing particle formation conditions, precursors, chemical composition, prevailing conditions, and sampling systems.

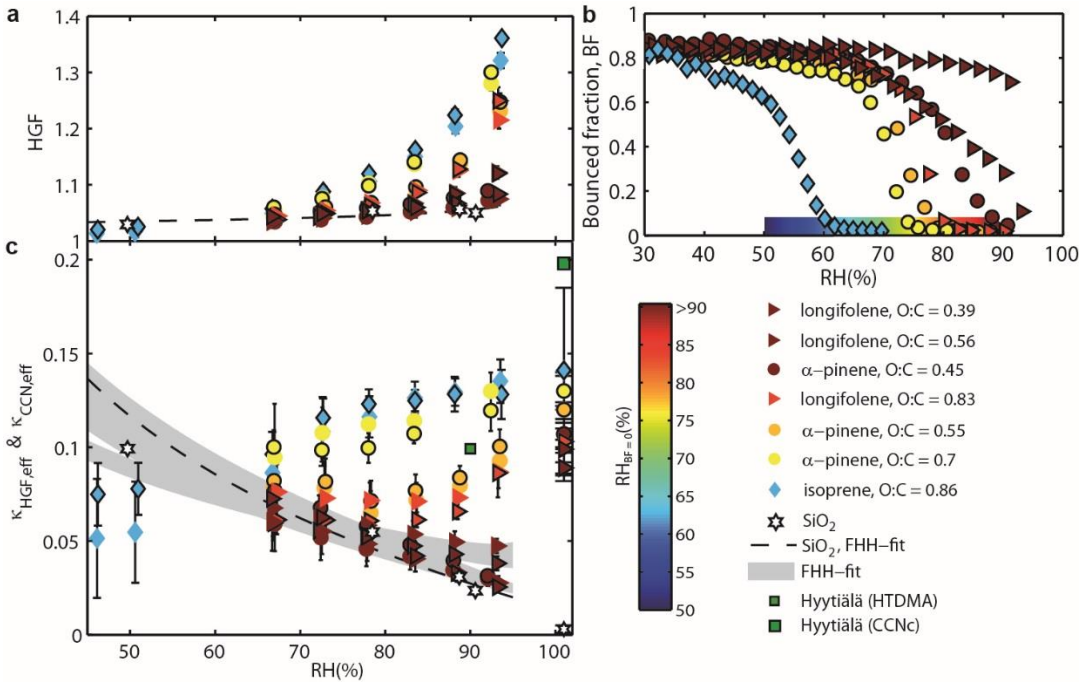

Figure 4.2. | Hygroscopic behavior of laboratory generated SOA particles, described using results from HTDMA, CCNc and ABI measurements. Spheres represent α-pinene, triangles longifolene, and diamonds isoprene SOA particles. Panel **a** shows the measured HGFs as a function of RH. Mobility diameters, d_p, of the SOA particles, 50 nm (without edge color) and 100 nm (black edges), and 50 nm for SiO_2 (white stars), are plotted. The colors of the data points represent the RH values where the bounced fraction falls to zero, as shown in panel **b** (i.e., for isoprene the zero point is RH ~62%, whereas for α-pinene with lowest O:C the zero point is RH ~92%). Panel **c** shows the hygroscopicity parameters calculated from HTDMA and CCNc data. The gray area represents FHH isotherms fitted to the data, and the green rectangles represent ambient data (d_p = 100 nm) measured in spring 2013 at the SMEAR II station in Hyytiälä, Finland (see SI in **Paper II**).

Phase transition linked with hygroscopicity. ABI, CCNc, and HTDMA were simultaneously employed in **Paper II** and the hygroscopicity-κ was calculated according to the principles introduced in Petters and Kreidenweis (2007) at varied RH (see eq(14)). Both GF and κ are shown for all the studied SOA particles in Fig 4.2. a and c, respectively. Overall, the κ values at the subsaturation regime are lower than the corresponding κ values measured with CCNc (at SS = 0.2%) and all the κ values are relatively low, always less than 0.15 (corresponding GF range of 1.07 – 1.37 at RH ~90%). These values are consistent with previous studies (Jimenez et al. 2009; Massoli et al. 2010). Because κ implicitly assumes a completely soluble phase, which may not be the case, we name our calculated κ values as "effective", κ_{eff}. However, all the SOA particles were assumed to be fully soluble in supersaturation conditions (Chap. 3.2.2.; CCNc). Thus, an average molecular weight of the particles

was calculated based on the CCNc measurements (assuming average molecular weight to be representative for all SOA mass) and the resulting molecular weights were used in the $\kappa_{HGF,eff}$ equation and Kelvin-term therein (eq(11)).

When taking a closer look at the data (Fig. 4.2.c), the κ trends, as a function of RH, form three distinct groups:

1) linearly decreasing κ with RH (dark brown data points)
2) increasing but leveling κ with RH (yellow and blue data points)
3) u-shape κ over RH range (orange and red data points)

As can be seen in Fig. 4.2., where the points were color-coded according to the liquefying RH (RH where BF reaches zero, i.e., $RH_{BF=0}$) gained from bounce measurements, these groups are clearly related to the bounce behavior of the particles. SOA particles which stay semisolid even at RH>85% belong to group 1, whereas the SOA particles which undergo phase transition already at RH<70% are in group 2. The SOA particles with u-shape (RH, κ) –relation are at the intermediate phase transition RH range, i.e., 70% < $RH_{BF=0}$ < 85% (see Fig. 4.2c).

To compare the water uptake of particles belonging to group 1 to the well-known adsorptive water uptake behavior of solid insoluble particles, we measured the hygroscopic GFs for SiO_2 particles (white stars in Fig. 4.2. a and c), which display similar trends (Fig. 4.2c) (Keskinen et al. 2011). Because the solid SiO_2 particles can take up water only via surface adsorption (Hertl and Hair, 1969), this suggests that a similar mechanism occurs for semisolid or sparingly soluble SOA particles, where the apparent hygroscopic growth is due to the surface adsorption of water rather than bulk water absorption. The adsorptive water uptake can be quantified with additional FHH-term in κ theory (eq(18)). The theory was fitted iteratively to the measured GF data of group 1 to derive the FHH parameters A_{FHH} and B_{FHH}. The area formed by fitted FHH isotherms is colored in grey in Fig. 4.2c. As can be seen, the FHH isotherm theory agrees well for the cases where the particles have stayed semisolid even at high RH (i.e., brown data points). These (RH, κ) –curves have a negative slope (group 1). As a comparison, the slope of theoretical κ-curve is 0. Thus, in terms of water uptake, it denotes that in FHH the adsorption water content is higher than expected based on the ideal κ at dry conditions, and lower at high RH.

FHH adsorption isotherms fitted to the data of group 1 correspond to ~20 water layers (one water layer being 0.28 nm) on the top of the SOA particles (100 nm) at RH~90%. The number of water monolayers is a realistic amount of water on the hydrophilic particle surface attached by adsorption. Birstein et al. (1955) observed ~60 layers of water adsorbed on lead and silver iodide particles at 75%RH and ~200 layers at 95%RH. Ma et al. (2010) observed ~15 layers of adsorbed water on Al_2O_3 particles at 95%RH and Sumner et al. (2004) observed 13 layers on halocarbon wax particles at 81%RH. Tadros et al. (1974) investigated contact angle and adsorption and observed ~23 monolayers of water at 95%RH on pyrolytic carbon surfaces. All of these particles are water-insoluble. In **Paper II**, we also covered the possibility that small quantities of SOA would dissolve into the adsorption layer in the low O:C SOA cases. Kumar et al. (2011) presented a model describing insoluble particles having a fraction of soluble material on their surface (eq(20) & eq(21)). Based on our calculations, with around 6% volume fraction

($\varepsilon_s = V_s/V_{tot}$) (corresponding 0.5 nm layer) of water soluble material, this reproduces already significantly different κ-slope compared to the observed behavior. This indicates that the fraction of the soluble material needs to be minor. Hence, it is possible that a minor part of the particles is dissolving at sub-saturation, but still adsorption dominates the water uptake process of the particles.

Ruehl et al. (2012) studied the effect of surface tension on SOA water activity. Based on our analysis, the κ values reported in **Paper II** are very insensitive to surface tension σ as it is associated only with the Kelvin term of the κ-Köhler equation (eq(25)). To demonstrate the insensitivity, we plotted the calculated κ values using two different values for σ (σ =0.072 N m^{-1}, equal to pure water, and 0.035 N m^{-1}, which is the lowest value reported for α-pinene SOA) in the Supplementary Information of **Paper II**. These values represent the limits of a reasonable range of surface tension of pure SOA particles (Wex et al. 2009). As is evident from the figure, varying the surface tension by a factor of two does not change the calculated $\kappa_{HGF,eff}$ values significantly.

Groups 2 and 3 are not modeled in **Paper II,** but plausible explanations for curve-like κ-slopes are discussed. The increasing trend (group 2) indicates that sparingly soluble compounds exist in the particle phase, which then dissolve gradually into water as the RH is increased. These observations indicate that isoprene SOA and highly oxidized α-pinene SOA liquefy at lower water activities, because they consist of compounds with a higher solubility. It is also highly possible that there is a solubility distribution of the compounds comprising SOA formed in each experiment. In that case, larger and larger fractions of the compounds dissolves with the increasing RH, causing an increasing $\kappa_{HGF,eff}$ with increasing RH. The behavior of group 3 (α-pinene SOA with O:C = 0.55 and longifolene SOA with O:C = 0.83) holds the influences of both group 1 and 2; at low RH, the particles stay semisolid and the water uptake is controlled by adsorption (i.e., slightly increased $\kappa_{HGF,eff}$). At higher RH, the sparingly soluble compounds start to dissolve into water one after another, which causes the increasing κ-slope at higher RHs.

A closer comparison between the HTDMA and CCNc results reveals that the differences in $\kappa_{HGF,eff}$ and $\kappa_{CCN,eff}$ are smallest for the particles that dissolve at lower RH (i.e., group 2) and largest for the particles exhibiting adsorption-dominated water uptake over the entire HTDMA measurement range (group 1). Our study suggests that $\kappa_{HGF,eff} < \kappa_{CCN,eff}$ because of adsorption-dominated water uptake by amorphous semisolid SOA particles in subsaturation conditions when the SOA is partially oxygenated. Petters et al. (2009) previously suggested that the observed $\kappa_{HGF} < \kappa_{CCN}$ discrepancy is caused either by a strongly composition-dependent activity coefficient of water or by a mixture of infinitely water-soluble compounds and sparingly soluble compounds that dissolve in solution at RH>90%.

4.1.3 Evaporation kinetics of α-pinene SOA particles

The evaporation of SOA particles was investigated in **Paper IV** in order to better understand the influence of the particle phase state on their evaporation kinetics. Hindered evaporation due to diffusion limitations in the particle phase could be seen as a slower evaporation than expected in the case of liquid particles. As shown above, α-pinene ozonolysis SOA particles have low, liquid-like, viscosity at RH ~80% (Renbaum-Wolff et al. 2013, **Paper II**) whereas dry, they are amorphous solids

(Zhang et al. 2015, Song et al. 2015). This is why the α-pinene ozonolysis SOA particles were chosen for the studies in **Paper IV** and the evaporation measurements were performed both when dry and at higher than RH = 80%.

The measurement results and the modeling results are shown in Fig. 4.3. As can be seen in panels a) and b), the SOA particles do shrink depending on the time (x axis) and RH in the tank, and the final fraction of the initial diameter asymptotically levels off towards a certain ratio. When comparing results between different evaporation RHs, it can be seen that the evaporation curve follows the same trend for RH ~40% (rectangles in Fig. 4.3. b) and RH ~80% (triangles in Fig. 4.3. a & b) (within measurement accuracy) but in the dry conditions (spheres in panel a), the evaporation is clearly slower. The evaporation results measured at dry conditions agree well with the previous results reported by Vaden et al. (2011), where the particles were formed in a Teflon chamber, 125 nm – 414 nm sized particles were studied, and the evaporation took place in a separate clean reactor.

It is noteworthy that in all cases the evaporation was clearly slower than expected based on the VBS previously determined for similar α-pinene SOA growth experiments (Pathak et al. 2007), assuming fully mixed liquid particles (illustrated in **Paper IV** and in Fig. 1. therein). Hence, we needed a revised VBS for the modeling. The evaporation at 80%RH could be modeled assuming fully mixed liquid particles (i.e., negligible diffusional limitations) while in dry conditions, the phase state could have an effect on evaporation rates. In **Paper IV**, we simulate an evaporation of SOA particles using two models. One assumes well-mixed liquid-like particles (a similar model as presented by Lehtinen and Kulmala, 2003) while the other, the Kinetic multi-layer model for gas-particle interactions in aerosols and clouds (KM-GAP), can simulate the evaporation of semisolid SOA particles (Shiraiwa et al. 2012).

Since the SOA formation was kept similar in all cases (i.e., different RHs), the initial SOA composition (t = 0) remained the same regardless of the evaporation-RH. The initial 1D-VBS can be derived for formed SOA (all cases) using the evaporation data measured at RH ~80% (liquid-like particles). For the liquid-like SOA particles case (RH ~80%), we used the VBS approach where a complicated organic system is simplified and presented by VBS of eight volatility bins, and used the genetic algorithm to find the optimal VBS bin distribution which would produce the best fit between a detailed evaporation model simulation and the measured SOA particle evaporation of the wet (RH ~80%) particle evaporation along the residence time. The tuning parameters for the model fitting were VBS bins representing the dry composition of the particles at the exit of the DMA1 (i.e., "initial VBS" or $VBS_{t=0}$). In order to capture the observed evaporation behavior, $VBS_{t=0}$ distribution needed to be shifted towards less volatile bins compared to VBS distribution reported by Pathak et al. (2007). The resulting best fit curve is colored red in Fig. 4.3. b) with the initial VBS in panel e), and the time-dependent evolution of VBS distribution is shown in **Paper IV** and Fig. 1. therein. We produced also an optimal "initial VBS", assuming an intentionally incorrect phase state (i.e., liquid) for the dry and 40%RH cases to emphasize the effect of the used assumptions about the phase state on resulting VBS. These $VBS_{t=0}$ distributions are shown in Fig. 4.3., panels c) and d). The difference between $VBS_{t=0}$ at dry and 80% RH conditions is clear; the initial VBS distribution is shifted to the lowest end of the utilized eight-bin VBS space at dry. For 40% RH the difference compared to 80% RH is less

pronounced. Such differences in the effective VBS derived at varying RH could be explained by increase in oligomer decomposition rate with RH.

KM-GAP was utilized when simulating the particle evaporation in dry and RH ~40% conditions (semisolid/solid cases). The particle-phase composition ($VBS_{t=0}$, see Fig 4.3e) was determined from the wet (RH ~80%) experiment and the particle-phase diffusion coefficient was calculated based on the viscosity using the Stokes-Einstein relation. Using constant viscosity, we cannot capture the measured particle evaporation (see Fig. 4.3. a), red, blue and green dashed curves). Instead of using constant viscosity, we let the viscosity vary along the evaporation (using eq(11)) from initially approximately 10^5 Pa s (or lower) and approaching finally around 10^8 - 10^9 Pa s (see dashed grey curves in Fig. 4.3. a) and b)). This viscosity range agrees well with the values recently reported by e.g., Grayson et al. (2016), and it indicates that the least volatile species remaining in the particle-phase at the end of the evaporation are the bigger molecules (Koop et al. 2011). The overall evaporation behavior seems to be affected by viscosity when it is greater than ~10^6 Pa s.

Measured particle evaporation at RH = 40% is shown in Fig. 4.3.b) as purple circles. The evaporation levels off to a similar ratio compared to the evaporation at RH = 80%, except at the early stage of the evaporation (i.e., evaporation time shorter than 30 minutes). Based on Raoult's effect, with the same initial organic composition and with a different water mole fraction, x_w, the evaporation at a lower RH should be clearly faster. Hence, the unexpectedly small difference in evaporation behavior at RH ~40% and 80% may result from a) diffusion limitations at RH ~40% or b) uncertainties in estimating the amount of particulate water. Water content was either calculated based on ideal solution theory (eq(12)) or utilizing hygroscopic growth factors (HGF) from previous experiments (**Paper II**). These methods are represented as red and blue dashed curves in Fig. 4.3. b), respectively. As can be seen, by using the HGF approach, the model agrees better with the measured evaporation. However, the best match between the experimental data and the simulations was made by using composition-dependent (denotes time-dependent) viscosity.

Vaden et al. (2011) performed evaporation measurements at dry, utilized VBS derived from particle growth measurements, and came to the conclusion that the diffusion of the organic particle-phase molecules is kinetically limited due to the high viscosity of the SOA particles, while Roldin et al. (2014) suggested the influences of oligomer degradation and mass transfer limitations leading to hindered evaporation. Our results indicate that diffusion limitations due to the relatively high viscosity of the SOA particles may play a role in the evaporation process between RH ~0% and 40%. At RH ~40% and higher, the evaporational loss of particle mass was captured well by assuming the particles to be liquid-like and using fitted VBS distribution. The interpretation about the viscosity of the SOA particles agrees well with recent phase studies (Renbaum-Wolff et al. 2013, Grayson et al. 2016), except the measurements done at RH ~40%, which are inconsistent with the results reported in Wilson et al. (2015). They reported similar evaporation kinetics for α-pinene SOA particles between RH = 5% and RH = 50% and faster evaporation at RH=90%. This contradiction may be due to small differences in evaporation conditions or the particle formation process. In our study, the prevailing ozone and α-pinene gas-phase concentrations in the flow tube were rather high. The fitted VBSs agree with previous

dry conditions evaporation studies (Shrivastava et al. 2013). Our simulations do not take into account possible chemical reactions occurring in the particle phase, such as oligomer decomposition, which have recently been proposed to affect the evaporation rates (Cappa and Wilson, 2011). Instead, decomposition and other similar effects may be included effectively in our derived VBS distributions.

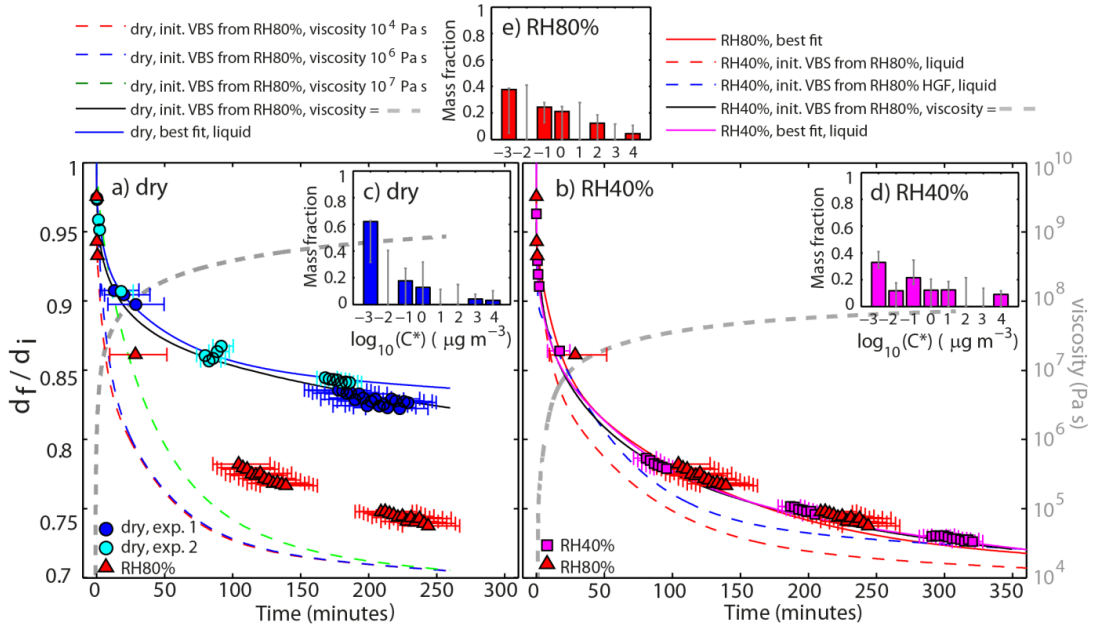

Figure 4.3. | Measurement results (data points) and model simulations for the evaporation of particles (d_i = 80 nm) under dry (a) and 40%RH (b) conditions while the 80% RH data is shown in both panels for comparison. The particle diameter with time normalized has the initial diameter d_i (a-b). Circles, squares and triangles show measured evaporation under dry (two experiments), 40% and 80% RH conditions, respectively. The model simulations in a: multi-layer model simulations for dry conditions using the best fit $VBS_{t=0,\ RH80\%}$ (i.e., initial VBS from the 80%RH experiment, see panel e) and assuming constant (dashed lines) or a composition-dependent particle viscosity (black solid line); well-mixed particle model simulation with the best fit initial composition for the dry 2 experiment (blue solid line). The model simulations in b: well-mixed particle model at 40%RH with the $VBS_{t=0,\ RH80\%}$ assuming an ideal solution (red dashed line); well-mixed particle model at 40%RH with water uptake calculated based on HGF (HGF = 1.01 at 40% RH) using the $VBS_{t=0,\ RH80\%}$ determined assuming HGF = 1.05 (blue dashed line); the multi-layer model at 40%RH with $VBS_{t=0,\ RH80\%}$ and assuming a composition-dependent particle viscosity (black solid line); the well-mixed particle model simulation with the best fit initial composition at 40%RH. Particle viscosities (dashed grey lines in panels a & b correspond to the model simulation shown with the black lines. The effective VBSs (panels c & d) show the best fit initial VBS distribution (bars) and variability within 20 genetic algorithm simulations (error bars) from the optimization of the well-mixed particle model (blue line in panel a) and purple line in panel b).

4.2 Physical properties of SOA particles in the atmosphere

Ambient SOA particles were assumed to be RH-independent and mainly liquid until 2010, when Virtanen et al. (2010) offered evidences that organic PM in a boreal forest of Northern Europe were amorphous semisolid or solid. The conclusion was made based on cascade impactor (ELPI) measurements conducted at dry RH. It was the first evidence of the existence of non-liquid submicron SOA particles in the atmosphere. Recently, Bateman et al. (2016) concluded that ambient SOA particles are primarily liquid in tropical forests in central Amazonia. Bateman et al.'s work (2016) was the first study to report a RH-dependent phase transition for amorphous ambient SOA particles. In this thesis, the major part of the measurements was done at real ambient conditions. In **Paper III** we report the physical and chemical properties of SOA particles measured in the Southeastern US, Alabama, including phase state measurements, while in **Paper II** the Hyytiälä ambient data from 2013 was used as a comparison data for the laboratory measurements.

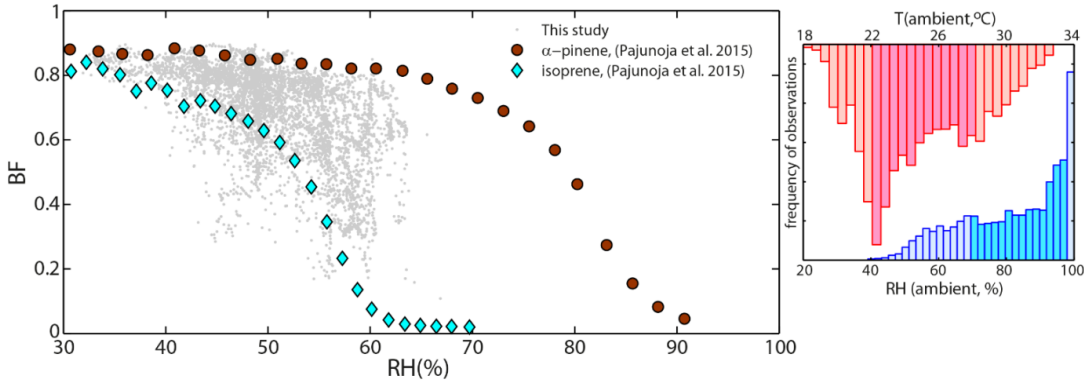

Figure 4.4. | Bounced fraction (BF) of the ambient SOA particles vs. RH in the ABI impactor (left), measured during the SOAS campaign. The bounce data is shown (grey dots) with the laboratory results recently reported in **Paper II** for α-pinene ozonolysis SOA (dark brown circles, O:C 0.56) and isoprene-derived SOA (light blue diamonds, O:C 1.07). Ambient conditions during the SOAS campaign (*T*; red bars and RH; blue bars) are shown in the subplot on the right hand side where the darker bars represent data within quartiles ($q_{25\%}$ and $q_{75\%}$).

In **Paper II,** we compare the reported laboratory results to real ambient observations conducted in early summer 2013 in boreal forest conditions in Hyytiälä, Finland. Sub- and supersaturation conditions similar to the laboratory measurements were used in the HTDMA and CCNc measurements. The campaign median hygroscopicity κ values are shown in Fig. 4.2b as green squares. A similar or even more pronounced discrepancy, namely $\kappa_{HGF} < \kappa_{CCN}$, can be seen (~0.1 and ~0.2, respectively) for ambient observations than in the laboratory SOA. Particle composition was derived by HR-ToF-AMS, resulting in the average organic fraction of 0.81 and O:C = 0.49, values which are also in the same range as the studied laboratory SOA. These results suggest that adsorptive water uptake and inhibited

hygroscopic growth in subsaturation conditions could take place also in the atmosphere. The atmospheric implications of this finding are discussed in next chapter (4.3.).

The phase transitions of ambient SOA particles were the main focus in **Paper III**. In ambient data, the contribution of inorganic species may complicate the analysis. While the mean mass fraction of organics was $f_{OA,mean}$ = 67% during the SOAS campaign, the ammonium bisulfate (ABS) was the second biggest contributor with mean mass fraction of f_{ABS} = 25%; sulfuric acid (SA) and ammonium sulfate (AS) mean mass concentrations were 7% and <1%, respectively. These fractions are based on AMS analysis to derive the mass fractions of organic and inorganic species and further categorization was made according to the method introduced in Nenes et al. (1998). The RH-dependent bounce data measured for ambient aerosol is shown in Fig 4.4. with grey dots (10min averages). As can be seen, the observed BF falls mainly between the BF curves measured for isoprene and monoterpene (α-pinene ozonolysis) SOA in **Paper II**. To investigate the phase state of OA fraction (f_{OA}), we limited the analysis to the data where f_{OA} was greater than 60%. This filtration removes the vast majority of the data points in the BF curve area fenced off by the laboratory data shown in Fig. 4.4.

According to the ABI measurements conducted during the SOAS campaign in Alabama, we can conclude that the phase transition from semisolid to liquid phase starts in the RH range from 40 to 60%, depending on the particle composition. At RH < 40%, the BF is always near the maximum (i.e., ~0.8 – 0.85), which indicates that the particles always consist of semisolid/solid material at dry RH. By increasing the RH over 40%, the BF starts to decrease, but it never reaches zero at RH <= 65%. We did not report any ABI measurements done at RH > 65% in **Paper III**. However, based on Bateman et al. (2015), the viscosity of SOA particles having approx. BF < 0.4 is already low enough to assume the liquid-like behavior of particles when atmospheric processes are considered. At higher RH, most of the BF data would be in the range of 0–0.1 and thus, any correlation between other parameters with BF could not be seen. Ambient T and RH are shown in Fig. 4.4. As can be seen, 75% of the time of the campaign, the ambient RH was greater than 70% and T > 22°C. By extrapolating the observed BF data according to previously studied SOA BF-curves (e.g., **Paper II**), the data indicates that the organic dominated ambient SOA particles are primarily liquid in the Southeast US in atmospherically relevant summertime conditions (RH, T), but they often turn semisolid when dried in the measurement setup below ~50%RH.

Phase transition of ambient particles linked with their κ and O:C. The links between O:C, hygroscopicity κ, f_{OA}, and the BF of the ambient aerosol particles were illustrated by color coding the measured (RH, BF) data with the listed parameters. HTDMA was employed in **Paper III** and the hygroscopicity-κ was calculated based on Petters and Kreidenweis (2007) at fixed RH = 90±3% (eq(25)). In addition, the hygroscopicity-κ was calculated for OA fraction only (κ_{OA}) by using the mixing rule (eq(27)). In the mixing rule, literature κ values for well-known inorganic species existing in the particle phase were used. O:C and f_{OA} were derived based on AMS analysis. As mentioned above, only the periods where f_{OA} > 0.6 were included in the analysis. In addition, rainy days (precipitation > 1 mm h^{-1}) were filtered from the analysis.

The color scaled plots are shown in Fig. 4. in **Paper III**. The results are in good agreement with earlier studies of the RH-dependent phase state of inorganic particles (e.g., Saukko et al. 2015) and OA species (e.g., **Paper II**); as OA fraction reaches ~0.8 (or higher), the BF remain higher than in the cases where $0.6 < f_{OA} < 0.8$. When linking the κ_{tot} with BF, it can be seen that the hygroscopicity (at RH ~90%) increases at times when the organic fraction is in the lower end (i.e. < 0.7). f_{OA} and κ_{tot} result from totally different measurement techniques (i.e., AMS and HTDMA, respectively) but still, support the observed bounce behavior. That is, when BF hits the highest BF-curve, typically f_{OA} also reaches the highest values and κ_{OA} is at the lowest level. The plot colored by κ_{OA} (Fig. 4d in **Paper III**) reveals that not only the inorganic fraction, but also the hygroscopicity of OA fraction is higher when the fraction of inorganics is the highest. This indicates higher water uptake, consequently more liquid-like particles, and thus, lower BF. The behavior of κ_{OA} is supported by O:C analysis; when κ_{OA} is the highest, O:C is the highest as well. The connection between κ_{OA} and O:C is reported previously based on measurements conducted in laboratory (e.g., Massoli et al. 2010), boreal forests (e.g., Raatikainen et al. 2010), during the SOAS campaign (Cerully et al. 2015), and in other locations (Jimenez et al. 2009). However, the (RH,BF) data colored with O:C do not show such a clear difference between the lowest and highest BF-curves.

The connections between these parameters were tested also by utilizing a structural equation modeling (e.g., Kline et al. 2015) analysis to show the total, direct and indirect effects of the predictor variables on BF. SEM analysis confirms the direct effect pathway of RH and κ_{tot} on BF while f_{OA} and κ_{OA} have indirect effects on BF. O:C has an influence both directly and indirectly (via κ_{OA}) on BF.

In terms of real ambient observations, to our knowledge, no other studies have reported linkage between the phase state and O:C. Bateman et al. (2016) compared hygroscopicity to their reported liquefying RH (BF reaches 0) and found good agreement (i.e., HGF ~1.10 at RH where BF = 0) with the laboratory studies (Bateman et al. 2015). They suggest that in an ambient condition where SOA particles are wetted such that their HGF > 1.10, the particles can be assumed to behave like liquid particles. This needs to be investigated in various sites in the real atmospheric conditions.

4.2.1 Effect of extended oxidation on SOA phase state (SOAS study)

Further OH oxidation of ambient SOA particles by the OFR provides a wider oxidation range for the analysis. Oxygenation has been shown to change properties of SOA with time (Ng et al. 2011). In **Paper III**, five stepped oxidation levels were used by varying the UV light intensity to simulate longer "effective aging times", up to three weeks. The lowest OH exposures increased the organic mass and also the O:C of f_{OA} slightly, whereas the higher OH exposures resulted in a clearly higher O:C, a loss of organic mass, and hence an increased mass fraction of ammonium bisulfate (f_{ABS}). According to the bounce measurements, the increased OH exposure decreased the phase transition RH (i.e., lowered the BF curve). This is emphasized at the highest OH exposures. After the OFR treatment, the correlation between BF and O:C is much more pronounced. O:C increases up to ~1.6. As showed in Fig 5. in **Paper III**, with the highest OH exposures, the O:C reaches the highest range, while BF values are at significantly lower level compared to the ambient observations. This is probably due to the increased hygroscopicity with increasing O:C.

4.3 Implications of the results

SOA studies need to be linked with atmospheric observations and the relevancies of the methods, models and conclusions must be critically overlooked. This thesis consists of multiple angles, mainly in the study of the physical properties of the atmospheric relevant SOA particles. The main idea is to increase our knowledge on the actual properties playing a major role in controlling particles' lifetimes in the atmosphere. The aerosol radiative interaction calculations reported in **Paper II** highlight the possible effect of a non-ideal water uptake mechanism on how ambient aerosols scatter sunlight directly.

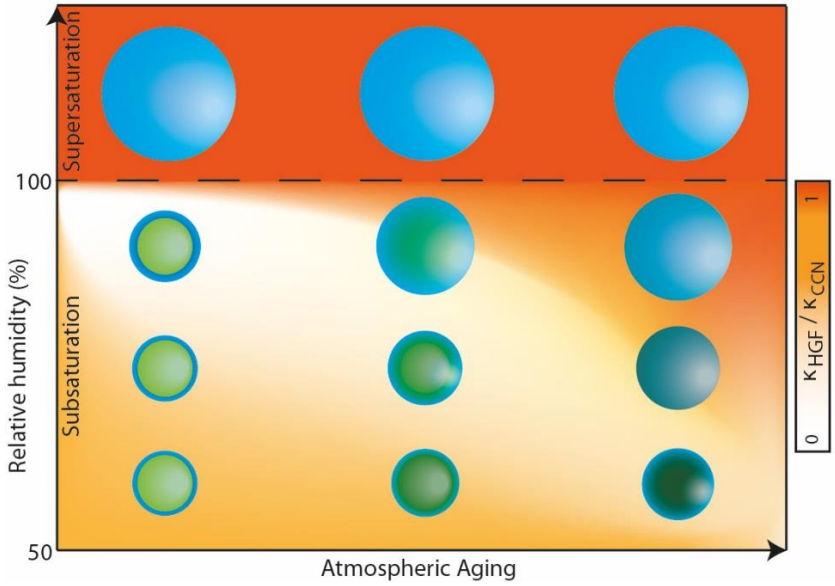

Figure 4.5. | Schematics of the water uptake processes of SOA particles in the atmosphere. Subsaturated swelling (κ_{HGF}) can vary dramatically with minor differences in supersaturated droplet activation (κ_{CCN}); consequently particles can have very different direct and indirect climate effects. The background color scale indicates the ratio of these parameters at given sub- and supersaturated conditions, whereas the darkness of the green color in the particles denotes their atmospheric age. The contrast is largest when adsorption is the dominant water uptake mechanism, even at high RH. This is the case for the low O:C SOA particles, on the left. With increasing oxidation, i.e., the increasing atmospheric age of the particles, the solubility increases and the dissolution-RH decreases. This decreases the discrepancy between the κ_{HGF} and κ_{CCN} values.

The schematic of the adsorptive water uptake of SOA particles in the atmosphere is shown in Fig. 4.5. The interpretation is based on the ratio between hygroscopicities measured at sub- and supersaturation

(background color in Fig. 4.5.). A ratio of one would denote ideal water uptake (dissolution) regardless of RH conditions, while lower ratio values would denote lowered water uptake ability at subsaturation. Due to atmospheric aging (increased O:C), the solubility of the compounds increases as the discrepancy between the sub- and supersaturation hygroscopicity diminishes.

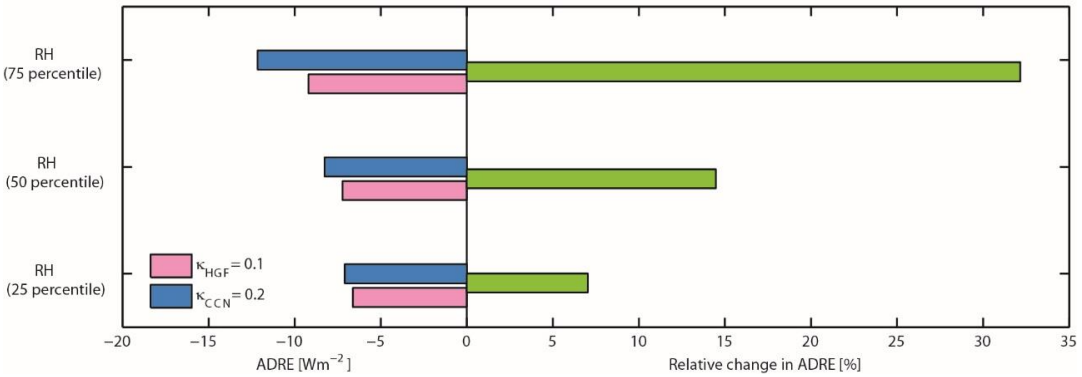

Figure 4.6. | Comparison of simulated Aerosol Direct Radiative Effect (ADRE) predicted from measured hygroscopicity κ values in Hyytiälä forest. ADREs [Wm^{-2}] calculated by the SBDART-model (see **Paper II** and its SI for details) are shown in the left panel for the two different total κ values measured in the campaign (κ_{HGF} = 0.1 and κ_{CCN} = 0.2, respectively). The relative change in ADRE [%] between the different κ is shown on the right-hand side (see SI of **Paper II**).

In terms of the hygroscopicity of SOA particles in the climate models, we want to emphasize the importance of the employed assumptions. If the particles are assumed to act as ideal solutions, the discrepancy (difference between κ_{HGF} and κ_{CCN}) can be assumed to be negligible. However, our study shows that this is not always the case, but hygroscopicity at subsaturation can be clearly lower. Adsorptive water uptake changes the wet size of the particles but it also can change their optical properties. Adsorbed monolayers of water on the particle surface could change the particles' abilities to scatter (and absorb) light directly in the atmosphere. However, this was not studied in detail in this thesis. Instead, in **Paper II**, we estimate the effects of a lowered κ-ratio on the aerosol direct radiative effect (ADRE) on the top of the atmosphere (TOA). This was performed for the data of ambient observations measured in the early summer 2013 at the SMEAR II station in Hyytiälä, Finland. In the model calculations, we used typical vertical aerosol particle concentration distribution, average particle number size distribution observed at ground level, estimated atmospheric conditions (ambient RH, P, T), and the measured average hygroscopicities of κ_{HGF} = 0.1 and κ_{CCN} = 0.2. The key point is that in many widely used atmospheric models, only a single value is employed to represent hyroscopicity at both sub- and supersaturation, and typically, κ_{CCN} is chosen to describe water uptake of ambient aerosols also below saturation point. By using the values separately in the ADRE model and by calculating the relative difference in these two cases, we are able to estimate the possible impact of utilizing "false" κ_{HGF} in the current ADRE models. The comparison of the simulated ADRE predictions

is shown in Fig. 4.6. In the median case, the relative difference is around 15%, while the quartiles show the possibility of having up to around 32% difference when using false κ_{CCN} instead of κ_{HGF}. Thus, the assumptions made on the particle hygroscopicity clearly affect the estimates of the direct radiative effects of SOA particles in the atmosphere.

One of the very first direct ambient measurements of the phase state of SOA particles conducted in the Southeastern US (**Paper III**) indicated that the viscosity of the particles is low enough to assume that they will behave like liquid particles in the atmosphere. Observations of highly viscous SOA particles in this area are still possible when ambient RH is in its lower end (i.e., < 50%) or if the particles are dried prior to the measurements. Similar conclusions are drawn in Bateman et al. (2016) about ambient aerosols over the Amazonian forest. Both studies suggest no limitations for the water uptake of the ambient particles, but discuss the possible diffusion limitations for huge oligomerized condensable organics (e.g., extremely low volatile compounds, dimers and trimers, Ehn et al. 2014). These studies highlight the dynamic role of SOA composition on their influence on the climate.

The laboratory results reported in this thesis indicate that SOA particles derived from biogenic precursors are highly viscous at dry conditions (**Paper I, II, IV**). As viscosity decreases with *T* and RH, the viscosity can play a role especially in atmospheric processes that take place in cold and/or dry areas. Based on the laboratory evaporation measurements reported in **Paper IV,** we concluded that at conditions relevant to warm ambient conditions, where the monoterpenes dominate the gas-phase VOC concentration (e.g., boreal forest where T ~20^{o}C and RH > 40%), the gas-particle mass transfer of organic compounds (molar mass ~150g/mol) is not delayed by highly viscous particle material. Instead, we highlight the importance of deriving accurate VBS to represent atmospheric organic constituents. As a summary, the probability of observing highly viscous SOA particles could increase i) spatially in polar climate regions, especially in a boreal forest environment where particulate mass is dominated by partially oxygenated SOA, and ii) vertically by moving from ground level towards the upper troposphere (*T* and RH decreases).

5. Author's contribution

The measurements reported in **Paper I** and **IV** were carried out at the aerosol laboratory (Department of Applied Physics) at the University of Eastern Finland. The results published in **Paper II** are based on laboratory measurements taken at the Chemistry Faculty at Boston College and the field measurements at the SMEAR II station in Hyytiälä (Finland), while the measurements of **Paper III** were organized by SOAS collaboration at a rural weather station in Centreville, Alabama, in the Southeastern US. I was involved all of the measurement campaigns, being primarily responsible for the ABI and/or HTDMA measurements.

Paper I is one of the very first studies to report a viscosity range for dry biogenic SOA particles produced in well-controlled laboratory conditions. K.E. Lehtinen and A. Virtanen brainstormed the initial plan for the paper. I analyzed, interpreted and visualized the data with the help of the co-authors. J. Malila and I were responsible for writing the paper, but all authors contributed to the writing.

Paper II investigates the RH-dependent water uptake of SOA particles which are formed in a PAM chamber. It shows that adsorption can be a plausible water uptake mechanism for fresh SOA particles. I developed and built the ABI for the campaign and took part in the planning of the project. During the campaign, A. Lambe took charge of the general measurement set-up while J. Hakala and I were responsible for the HTDMA and the ABI measurements respectively. I combined and visualized the data from all instruments and interpreted the data with the assistance of the co-authors. I had a main responsibility in the paper writing, but all the authors contributed to the writing of the paper.

Paper III reports the results from real ambient observations measured in the southeastern US. The analysis focuses on the linking phase state of organic dominated atmospheric organic aerosols to their hygroscopicity and organic fraction. Furthermore, the influence of chemical aging of the particles on their physical properties is investigated by sampling the particles through a OFR. The HTDMA measurements were carried out by the group under the supervision of D.Collins, and the AMS data were collected (and processed) mainly by the research group of J.Jimenez. I modified the ABI to be applicable for challenging ambient conditions and conducted the ABI measurements at the site. I combined the data from all the instruments and interpreted the data with the assistance of the co-authors. I had a main responsibility in the paper writing, but all the authors contributed to the writing.

Paper IV presents the particle evaporation analysis for the SOA particles formed in a flow tube. The paper shows how the viscosity affects the evaporation rate of the particles at dry conditions whereas at RH>40% the evaporation can be modelled well by assuming the particles to be fully liquid. I was mainly responsible for designing and conducting the first set of the measurements, took part in the data interpretation and analysis, and made a minor contribution to the writing.

6. Summary

This thesis relates the phase changes of biogenic SOA particles to their hygroscopic properties, chemical composition, degree of oxidation, and gas-phase precursor properties. The measurements were conducted in laboratory for the SOA particles formed via the oxidation of single precursor VOC gases, as well as in field conditions at regions where the same precursor VOCs have been shown to hold a dominant role in the SOA formation. The findings of the thesis significantly increase our understanding of one of the most relevant atmospheric processes involving organic aerosols: water uptake. The conclusions also reconcile previously described differences between the hygroscopicity of SOA measured in subsaturated and supersaturated conditions. The main conclusions of this thesis are as follows:

1) Submicron biogenic SOA particles are typically semisolid or even glassy at dry conditions at room temperature.

SOA particles originating from real pine-VOC emissions can have a viscosity greater than 10^{12} Pa s at dry conditions while the viscosity of the SOA particles formed from the ozonolysis of pure α-pinene is lower, in the order of 10^{8} Pa s. These conclusions were made based on particles' morphological changes and coalescence time analysis. Our results are one of the first viscosity estimations for nanoscale biogenic SOA particles and to our knowledge, the first viscosity study with respect to real pine-VOC derived SOA particles.

According to our comprehensive bounce dataset collected both in the laboratory and during the field campaigns, it is indicated that atmospherically relevant SOA particles from biogenic precursors are composed of semisolid material at RH < 30%. No evidence on liquid-like SOA particles in dry conditions during the SOAS campaign that took place in the Southeastern US was found.

2) Oxidative aging tends to increase the hygroscopicity of amorphous solid SOA particles that can be detected at high RH. It also tends to decrease the transition RH where the particles liquefy.

During the work presented in this thesis, we built an improved tool (ABI) to measure the particle bounce of SOA particles at wide RH range. With the help of the ABI, we were able to detect the exact RH where the particles undergo the phase transition from semisolid into liquid. The ABI measurements were not sensitive enough to capture the effect of O:C on the viscosity of the dry particles. Instead, RH-dependent viscosity of the particles was analyzed at elevated RH. According to the laboratory studies, the liquefying RH of the SOA particles formed from single precursor gas decreases with increasing O:C and with the decreasing molecular weight of the precursor VOC. Ambient observations support the finding of the link between particles' liquefying RH and O:C, though the effect is not that evident.

3) Water uptake mechanism and evaporation kinetics can be influenced by the semisolidness of the SOA particles.

Our results show that for subsaturated conditions, the water uptake of the SOA particles with relatively low O:C (i.e., fresh SOA) can be an adsorption-dominated process. The viscosity of the particles is not a key factor causing restricted uptake of water, but low solubility inhibits the miscibility and hence, the

water uptake and semisolidness until the RH is high enough for dissolution to occur. With increasing O:C, the solubility increases, the dissolution RH decreases, and the hygroscopicity at subsaturation closes in on the hygroscopicity measured in supersaturation conditions.

Regardless of the negligible diffusional limitations of water molecules in the SOA matrix (of the order of atmospheric relevant timescales), the evaporation/condensation of larger organic molecules may still be kinetically limited. Based on our findings, the evaporation of fresh SOA particles formed via ozonolysis of α-pinene is slower than expected at dry conditions, partly due to their high viscosity. Nonetheless, the viscosity effect diminishes already at RH ~40% (at room T). To capture the evaporation rate of the SOA particles with the model, the volatility distribution representing the α-pinene SOA particles needs to be shifted to lower saturation concentrations than previously reported. The best match between the simulations and evaporation experiments is reached if the viscosity is increased with residence (during evaporation) time. Chemical reactions in the particle phase were excluded in the modelling.

6.1 Future perspectives

Ambient temperature and RH establish a wide spatial and temporal variety of conditions in which the amorphous SOA particles undergo phase transitions. Increased viscosity can slow down particle-phase processes, ultimately inducing significant changes in particle composition. The vast majority of the phase state and diffusion studies of SOA particles have been conducted around room temperature (T ~298K) and hence they have replicated ambient conditions at ground level in summer season (except the polar region). Recent studies show that the uptake of water and oxidants by organic aerosols may not be kinetically hindered while the effect of viscosity on the mass transfer of more volatile organics requires more detailed investigations. In terms of the future direction of SOA research, forthcoming studies focusing on ground level processes should concentrate more on finding an accurate way to describe SOA composition (e.g., VBS approach), and link the improved methods with the latest viscosity (and diffusion coefficient) estimations. Ideally, future global climate models could parametrize η as functions of C^*, M_i, and O:C. The future phase state studies instead could take the next step in studying SOA particles in the upper troposphere and the processes therein (e.g., ice cloud activation), where temperatures can get as low as -56^{o}C (Seinfeld and Pandis, 2006) and the existence of glassy solid SOA particles is plausible. Even the uptake of water and the smallest trace gases could be influenced by the highly viscous particle phase in conditions similar to the upper troposphere.

As a technical note, future studies that report viscosity and/or the diffusion coefficient for SOA particles should clearly also report the formation and prevailing conditions (T, P, RH), as well as the chemical characterization of the particles (O:C and H:C or preferably representative VBS) alongside the main results. In terms of climate modeling and the estimation of climate effects, special attention should be paid to the κ values used in the calculation of ADRE or the CCN activation of atmospheric SOA particles.

References

Abramson, E., Imre, D., Beranek, J., Wilson, J. and Zelenyuk, A.: Experimental determination of chemical diffusion within secondary organic aerosol particles, Phys. Chem. Chem. Phys., 15, 2983-2991, 2013.

Attwood, A., Washenfelder, R., Brock, C., Hu, W., Baumann, K., Campuzano-Jost, P., Day, D., Edgerton, E., Murphy, D. and Palm, B.: Trends in sulfate and organic aerosol mass in the Southeast US: Impact on aerosol optical depth and radiative forcing, Geophys. Res. Lett., 41, 7701-7709, 2014.

Bateman, A. P., Belassein, H. and Martin, S. T.: Impactor apparatus for the study of particle rebound: Relative humidity and capillary forces, Aer. Sci. Tech., 48, 42-52, 2014.

Bateman, A. P., Gong, Z., Liu, P., Sato, B., Cirino, G., Zhang, Y., Artaxo, P., Bertram, A. K., Manzi, A. O. and Rizzo, L. V.: Sub-micrometre particulate matter is primarily in liquid form over Amazon rainforest, Nat. Geosci., 9, 34-37, 2016.

Berkemeier, T., Shiraiwa, M., Pöschl, U. and Koop, T.: Competition between water uptake and ice nucleation by glassy organic aerosol particles, Atmos. Chem. Phys., 14, 12513-12531, 2014.

Berthier, L., Biroli, G., Bouchaud, J., Cipelletti, L. and van Saarloos, W.: Dynamical heterogeneities in glasses, colloids, and granular media, Oxford, 2011.

Birstein S.J., The role of adsorption in heterogeneous nucleation, Adsorption of water vapor on silver iodide and lead iodide, J. Meteorology 12, 324-331, 1955.

Brock, C. A., Wagner, N. L., Anderson, B. E., Attwood, A. R., Beyersdorf, A., Campuzano-Jost, P., Carlton, A. G., Day, D. A., Diskin, G. S., Gordon, T. D., Jimenez, J. L., Lack, D. A., Liao, J., Markovic, M. Z., Middlebrook, A. M., Ng, N. L., Perring, A. E., Richardson, M. S., Schwarz, J. P., Washenfelder, R. A., Welti, A., Xu, L., Ziemba, L. D. and Murphy, D. M.: Aerosol optical properties in the southeastern United States in summer - Part 1: Hygroscopic growth, Atmos. Chem. Phys., 16, 4987-5007, 2016.

Cappa, C. D. and Wilson, K.: Evolution of organic aerosol mass spectra upon heating: implications for OA phase and partitioning behavior, Atmos. Chem. Phys., 11, 1895-1911, 2011.

Cerully, K., Bougiatioti, A., Hite Jr, J., Guo, H., Xu, L., Ng, N., Weber, R. and Nenes, A.: On the link between hygroscopicity, volatility, and oxidation state of ambient and water-soluble aerosols in the southeastern United States, Atmos. Chem. Phys., 15, 8679-8694, 2015.

Clegg, S. L., Brimblecombe, P. and Wexler, A. S.: Thermodynamic model of the system H-NH_4 - $(SO_4)_2$-NO_3-H_2O at tropospheric temperatures, J. Phys. Chem. A, 102, 2137-2154, 1998.

De Carlo, P. F., Kimmel, J. R., Trimborn, A., Northway, M. J., Jayne, J. T., Aiken, A. C., Gonin, M., Fuhrer, K., Horvath, T., Docherty, K. S., Worsnop, D. R. and Jimenez, J. L.: Field-deployable, high-resolution, time-of-flight aerosol mass spectrometer, Anal. Chem., 78, 8281-8289, 2006.

Denjean, C., Formenti, P., Picquet-Varrault, B., Camredon, M., Pangui, E., Zapf, P., Katrib, Y., Giorio, C., Tapparo, A. and Temime-Roussel, B.: Aging of secondary organic aerosol generated from the ozonolysis of α-pinene: effects of ozone, light and temperature, Atmos. Chem. Phys., 15, 883-897, 2015.

Donahue, N. M., Epstein, S., Pandis, S. N. and Robinson, A. L.: A two-dimensional volatility basis set: 1. organic-aerosol mixing thermodynamics, Atmos. Chem. Phys., 11, 3303-3318, 2011.

Donahue, N., Robinson, A., Stanier, C. and Pandis, S.: Coupled partitioning, dilution, and chemical aging of semivolatile organics, Environ. Sci. Tech., 40, 2635-2643, 2006.

Donahue, N. M., Henry, K. M., Mentel, T. F., Kiendler-Scharr, A., Spindler, C., Bohn, B., Brauers, T., Dorn, H. P., Fuchs, H., Tillmann, R., Wahner, A., Saathoff, H., Naumann, K. H., Mohler, O., Leisner, T., Muller, L., Reinnig, M. C., Hoffmann, T., Salo, K., Hallquist, M., Frosch, M., Bilde, M., Tritscher, T., Barmet, P., Praplan, A. P., DeCarlo, P. F., Dommen, J., Prevot, A. S. and Baltensperger, U.: Aging of biogenic secondary organic aerosol via gas-phase OH radical reactions, Proc. Natl. Acad. Sci. U. S. A., 109, 13503-13508, 2012.

Dusek, U., Frank, G.P., Hildebrandt, L., Curtius, J., Schneider, J., Walter, S., Chand, D., Drewnick, F., Hings, S., Jung, D., Borrmann, S., and Andreae, M.O.: Size matters more than chemistry for cloud-nucleating ability of aerosol particles, Science, 312 (5778), 1375-1378, 2006.

Ehn, M., Thornton, J. A., Kleist, E., Sipilä, M., Junninen, H., Pullinen, I., Springer, M., Rubach, F., Tillmann, R. and Lee, B.: A large source of low-volatility secondary organic aerosol, Nature, 506, 476-479, 2014.

Finessi, E., Decesari, S., Paglione, M., Giulianelli, L., Carbone, C., Gilardoni, S., Fuzzi, S., Saarikoski, S., Raatikainen, T., Hillamo, R., Allan, J., Mentel, T. F., Tiitta, P., Laaksonen, A., Petaja, T., Kulmala, M., Worsnop, D. R. and Facchini, M. C.: Determination of the biogenic secondary organic aerosol fraction in the boreal forest by NMR spectroscopy, Atmos. Chem. Phys., 12, 941-959, 2012.

Friedlander, S. K.: Smoke, dust, and haze, Oxford University press, New York, 2000.

Frenkel, J.: Kinetic Theory of Liquids, Dover, New York, 1955.

Frenkel, J.: Viscous Flow of Crystalline Bodies Under the Action of Surface Tension, J. Phys. (Moscow), 9: 385–391, 1945.

Frosch, M., Bilde, M., Tritscher, T., Barmet, P., Praplan, A. P., DeCarlo, P. F., Dommen, J., Prevot, A. S. and Baltensperger, U.: Aging of biogenic secondary organic aerosol via gas-phase OH radical reactions, Proc. Natl. Acad. Sci. U. S. A., 109, 13503-13508, 2012.

Grayson, J. W., Song, M., Sellier, M. and Bertram, A. K.: Validation of the poke-flow technique combined with simulations of fluid flow for determining viscosities in samples with small volumes and high viscosities, Atmos. Meas. Tech., 8, 2463-2472, 2015.

Grayson, J. W., Zhang, Y., Mutzel, A., Renbaum-Wolff, L., Boege, O., Kamal, S., Herrmann, H., Martin, S. T. and Bertram, A. K.: Effect of varying experimental conditions on the viscosity of alpha-pinene derived secondary organic material, Atmos. Chem. Phys., 16, 6027-6040, 2016.

Guenther, A. B., Jiang, X., Heald, C. L., Sakulyanontvittaya, T., Duhl, T., Emmons, L. K. and Wang, X.: The Model of Emissions of Gases and Aerosols from Nature version 2.1 (MEGAN2.1): an extended and updated framework for modeling biogenic emissions, Geosci. Mod. Develop. 5(6): 1471–1492, 2012.

Gysel, M., Crosier, J., Topping, D., Whitehead, J., Bower, K., Cubison, M., Williams, P., Flynn, M., McFiggans, G. and Coe, H.: Closure study between chemical composition and hygroscopic growth of aerosol particles during TORCH2, Atmos. Chem. Phys., 7, 6131-6144, 2007.

Hallquist, M., Wenger, J., Baltensperger, U., Rudich, Y., Simpson, D., Claeys, M., Dommen, J., Donahue, N., George, C. and Goldstein, A.: The formation, properties and impact of secondary organic aerosol: current and emerging issues, Atmos. Chem. Phys., 9, 5155-5236, 2009.

Halsey, G.: Physical adsorption on non-uniform surfaces, J. Chem. Phys., 16(10), 931–937, 1948.

Hari, P. and Kulmala, M.: Station for measuring ecosystem-atmosphere relations (SMEAR II), Boreal Environ. Res., 10, 315-322, 2005.

Hertl, W. and Hair, M.L., Adsorption of water on Silica, Nature, 223, 1150-1151, 1969

Hill, T. L.: Physical adsorption and the free volume model for liquids, J. Chem. Phys., 17(6), 590–590, 1949.

Hinds, W. C.: Aerosol technology: properties, behavior, and measurement of airborne particles, John Wiley & Sons, 2012.

Hong, J., Häkkinen, S., Paramonov, M., Äijälä, M., Hakala, J., Nieminen, T., Mikkilä, J., Prisle, N., Kulmala, M. and Riipinen, I.: Hygroscopicity, CCN and volatility properties of submicron atmospheric aerosol in a boreal forest environment during the summer of 2010, Atmos. Chem. Phys., 14, 4733-4748, 2014.

Häkkinen, S. A. K., Äijälä, M., Lehtipalo, K., Junninen, H., Backman, J., Virkkula, A., Nieminen, T., Vestenius, M., Hakola, H., Ehn, M., Worsnop, D. R., Kulmala, M., Petäjä, T. and Riipinen, I.: Long-term volatility measurements of submicron atmospheric aerosol in Hyytiala, Finland, Atmos. Chem. Phys., 12, 10771-10786, 2012.

Järvinen, E., Ignatius, K., Nichman, L., Kristensen, T. B., Fuchs, C., Hoyle, C. R., Hoeppel, N., Corbin, J. C., Craven, J., Duplissy, J., Ehrhart, S., El Haddad, I., Frege, C., Gordon, H., Jokinen, T., Kallinger, P., Kirkby, J., Kiselev, A., Naumann, K., Petaja, T., Pinterich, T., Prevot, A. S. H., Saathoff, H., Schiebel, T., Sengupta, K., Simon, M., Slowik, J. G., Troestl, J., Virtanen, A., Vochezer, P., Vogt, S., Wagner, A. C., Wagner, R., Williamson, C., Winkler, P. M., Yan, C., Baltensperger, U., Donahue, N. M., Flagan, R. C., Gallagher, M., Hansel, A., Kulmala, M., Stratmann, F., Worsnop, D. R., Moehler, O., Leisner, T. and Schnaiter, M.: Observation of viscosity transition in alpha-pinene secondary organic aerosol, Atmos. Chem. Phys., 16, 4423-4438, 2016.

Jayne, J. T., Leard, D. C., Zhang, X., Davidovits, P., Smith, K. A., Kolb, C. E. and Worsnop, D. R.: Development of an aerosol mass spectrometer for size and composition analysis of submicron particles, Aer. Sci. Tech., 33, 49-70, 2000.

Jimenez, J. L., Canagaratna, M. R., Donahue, N. M., Prevot, A. S., Zhang, Q., Kroll, J. H., DeCarlo, P. F., Allan, J. D., Coe, H., Ng, N. L., Aiken, A. C., Docherty, K. S., Ulbrich, I. M., Grieshop, A. P., Robinson, A. L., Duplissy, J., Smith, J. D., Wilson, K. R., Lanz, V. A., Hueglin, C., Sun, Y. L., Tian, J., Laaksonen, A., Raatikainen, T., Rautiainen, J., Vaattovaara, P., Ehn, M., Kulmala, M., Tomlinson, J. M., Collins, D. R., Cubison, M. J., Dunlea, E. J., Huffman, J. A., Onasch, T. B., Alfarra, M. R., Williams, P. I., Bower, K., Kondo, Y., Schneider, J., Drewnick, F., Borrmann, S., Weimer, S., Demerjian, K., Salcedo, D., Cottrell, L., Griffin, R., Takami, A., Miyoshi, T., Hatakeyama, S., Shimono, A., Sun, J. Y., Zhang, Y. M., Dzepina, K., Kimmel, J. R., Sueper, D., Jayne, J. T., Herndon, S. C., Trimborn, A. M., Williams, L. R., Wood, E. C., Middlebrook, A. M., Kolb, C. E., Baltensperger, U. and Worsnop, D. R.: Evolution of organic aerosols in the atmosphere, Science, 326, 1525-1529, 2009.

Kanakidou, M., Seinfeld, J., Pandis, S., Barnes, I., Dentener, F., Facchini, M., Dingenen, R. V., Ervens, B., Nenes, A. and Nielsen, C.: Organic aerosol and global climate modelling: a review, Atmos. Chem. Phys., 5, 1053-1123, 2005.

Karnezi, E., Riipinen, I. and Pandis, S. N.: Measuring the atmospheric organic aerosol volatility distribution: a theoretical analysis, Atmos. Meas. Tech., 7, 2953-2965, 2014.

Kerminen, V., Lihavainen, H., Komppula, M., Viisanen, Y. and Kulmala, M.: Direct observational evidence linking atmospheric aerosol formation and cloud droplet activation, Geophys. Res. Lett., 32, L14803, 2005.

Keskinen, H., Romakkaniemi, S., Jaatinen, A., Miettinen, P., Saukko, E., Joutsensaari, J., Makela, J. M., Virtanen, A., Smith, J. N. and Laaksonen, A.: On-Line Characterization of Morphology and Water Adsorption on Fumed Silica Nanoparticles, Aerosol. Sci. Technol., 45, 1441-1447, 2011.

Kidd, C., Perraud, V., Wingen, L. M. and Finlayson-Pitts, B. J.: Integrating phase and composition of secondary organic aerosol from the ozonolysis of alpha-pinene, Proc. Natl. Acad. Sci. U. S. A., 111, 7552-7557, 2014.

Kline, R. B.: Principles and practice of structural equation modeling, Guilford publications, 2015.

Knutson, E. and Whitby, K.: Anomalous Unipolar Diffusion Charging of Polystyrene Latex Aerosols, J. Colloid Interface Sci., 53, 493-495, 1975.

Koop, T., Bookhold, J., Shiraiwa, M. and Pöschl, U.: Glass transition and phase state of organic compounds: dependency on molecular properties and implications for secondary organic aerosols in the atmosphere, Phys. Chem. Chem. Phys., 13, 19238-19255, 2011.

Kroll, J. H., Donahue, N. M., Jimenez, J. L., Kessler, S. H., Canagaratna, M. R., Wilson, K. R., Altieri, K. E., Mazzoleni, L. R., Wozniak, A. S. and Bluhm, H.: Carbon oxidation state as a metric for describing the chemistry of atmospheric organic aerosol, Nat. Chem., 3, 133-139, 2011.

Kroll, J. H. and Seinfeld, J. H.: Chemistry of secondary organic aerosol: Formation and evolution of low-volatility organics in the atmosphere, Atmos. Environ., 42, 3593-3624, 2008.

Kulmala, M., Vehkamaki, H., Petaja, T., Dal Maso, M., Lauri, A., Kerminen, V., Birmili, W. and McMurry, P.: Formation and growth rates of ultrafine atmospheric particles: a review of observations, J. Aerosol Sci., 35, 143-176, 2004.

Kulmala, M., Riipinen, I., Sipilä, M., Manninen, H.E., Petäjä, T., Junninen, H., Dal Maso, M., Mordas, G., Mirme, A., Vana, M., Hirsikko, A., Laakso, L., Harrison, R.M., Hanson, I., Leung, C., Lehtinen, K.E.J. and Kerminen, V-M.: Towards Direct Measurement of Atmospheric Nucleation, Science, 318, 89-91, 2007.

Kumar, P., Sokolik, I. N. and Nenes, A.: Cloud condensation nuclei activity and droplet activation kinetics of wet processed regional dust samples and minerals, Atmos. Chem. Phys., 11, 8661-8676, 2011.

Kumar, P., Sokolik, I. N. and Nenes, A.: Measurements of cloud condensation nuclei activity and droplet activation kinetics of fresh unprocessed regional dust samples and minerals, Atmos. Chem. Phys., 11, 3527-3541, 2011.

Kumar, P., Sokolik, I. N. and Nenes, A.: Parameterization of cloud droplet formation for global and regional models: including adsorption activation from insoluble CCN, Atmos. Chem. Phys., 9, 2517-2532, 2009.

Kumar, P., Nenes, A. and Sokolik, I. N.: Importance of adsorption for CCN activity and hygroscopic properties of mineral dust aerosol, Geophys. Res. Lett., 36, L24804, 2009.

Kuwata, M. and Martin, S. T.: Particle size distributions following condensational growth in continuous flow aerosol reactors as derived from residence time distributions: Theoretical development and application to secondary organic aerosol, Aer. Sci. Tech., 46, 937-949, 2012.

Kuwata, M. and Martin, S. T.: Phase of atmospheric secondary organic material affects its reactivity, Proc. Natl. Acad. Sci. U. S. A., 109, 17354-17359, 2012.

Köhler, H.: The nucleus in and the growth of hygroscopic droplets. Trans.Faraday Soc., 32, 1152–1161, 1936.

Laaksonen, A., Malila, J., Nenes, A., Hung, H. and Chen, J.: Surface fractal dimension, water adsorption efficiency, and cloud nucleation activity of insoluble aerosol, Sci. Rep., 6, 25504, 2016.

Lambe, A., Onasch, T., Massoli, P., Croasdale, D., Wright, J., Ahern, A., Williams, L., Worsnop, D., Brune, W. and Davidovits, P.: Laboratory studies of the chemical composition and cloud condensation nuclei (CCN) activity of secondary organic aerosol (SOA) and oxidized primary organic aerosol (OPOA), Atmos. Chem. Phys., 11, 8913-8928, 2011.

Lehtinen, K. and Kulmala, M.: A model for particle formation and growth in the atmosphere with molecular resolution in size, Atmos. Chem. Phys., 3, 251-257, 2003.

Lehtipalo K., Kulmala, M., Sipilä, M., Petäjä, T., Vana, M., Ceburnis, D., Dupuy, R. and O'Dowd, C.O..: Atmos. Chem. Phys., 10, 7009–7016, 2010.

Li, Y. J., Liu, P., Gong, Z., Wang, Y., Bateman, A. P., Bergoend, C., Bertram, A. K. and Martin, S. T.: Chemical Reactivity and Liquid/Nonliquid States of Secondary Organic Material, Environ. Sci. Tech., 49, 13264-13274, 2015.

Lienhard, D. M., Huisman, A. J., Bones, D. L., Te, Y., Luo, B. P., Krieger, U. K. and Reid, J. P.: Retrieving the translational diffusion coefficient of water from experiments on single levitated aerosol droplets, Phys. Chem. Chem. Phys., 16, 16677-16683, 2014.

Lienhard, D. M., Huisman, A. J., Krieger, U. K., Rudich, Y., Marcolli, C., Luo, B. P., Bones, D. L., Reid, J. P., Lambe, A. T., Canagaratna, M. R., Davidovits, P., Onasch, T. B., Worsnop, D. R., Steimer, S. S., Koop, T. and Peter, T.: Viscous organic aerosol particles in the upper troposphere: diffusivity-controlled water uptake and ice nucleation?, Atmos. Chem. Phys., 15, 13599-13613, 2015.

Lignell, H., Hinks, M. L. and Nizkorodov, S. A.: Exploring matrix effects on photochemistry of organic aerosols, Proc. Natl. Acad. Sci. U. S. A., 111, 13780-13785, 2014.

Liu, B., Pui, D., Whitby, K., Kittelson, D., Kousaka, Y. and McKenzie, R.: Aerosol Mobility Chromatograph - New Detector for Sulfuric-Acid Aerosols, Atmos. Environ., 12, 99-104, 1978.

Ma, Q, Liu, Y. and He, Hong, The Utilization of Physisorption Analyzer for Studying the Hygroscopic Properties of Atmospheric Relevant Particles, J. Phys. Chem., 2010.

Martin, S.: Phase transitions of aqueous atmospheric particles, Chem. Rev., 100, 3403-3453, 2000.

Massoli, P., Lambe, A., Ahern, A., Williams, L., Ehn, M., Mikkilä, J., Canagaratna, M., Brune, W., Onasch, T. and Jayne, J.: Relationship between aerosol oxidation level and hygroscopic properties of laboratory generated secondary organic aerosol (SOA) particles, Geophys. Res. Lett., 37 (24), 2010.

McCormick, M., Thomason, L. and Trepte, C.: Atmospheric Effects of the Mt-Pinatubo Eruption, Nature, 373, 399-404, 1995.

McFiggans, G., Artaxo, P., Baltensperger, U., Coe, H., Facchini, M. C., Feingold, G., Fuzzi, S., Gysel, M., Laaksonen, A. and Lohmann, U.: The effect of physical and chemical aerosol properties on warm cloud droplet activation, Atmos. Chem. Phys., 6, 2593-2649, 2006.

McMurry, P. and Stolzenburg, M.: On the Sensitivity of Particle-Size to Relative-Humidity for Los-Angeles Aerosols, Atmos. Environ., 23, 497-507, 1989.

Mikhailov, E., Vlasenko, S., Martin, S., Koop, T. and Pöschl, U.: Amorphous and crystalline aerosol particles interacting with water vapor: conceptual framework and experimental evidence for restructuring, phase transitions and kinetic limitations, Atmos. Chem. Phys., 9, 9491-9522, 2009.

Nenes, A., Pandis, S. N. and Pilinis, C.: ISORROPIA: A new thermodynamic equilibrium model for multiphase multicomponent inorganic aerosols, Aquat. Geochem., 4, 123-152, 1998.

Ng, N. L., Canagaratna, M. R., Jimenez, J. L., Chhabra, P. S., Seinfeld, J. H. and Worsnop, D. R.: Changes in organic aerosol composition with aging inferred from aerosol mass spectra, Atmos. Chem. Phys., 11, 6465-6474, 2011.

Nguyen, T., Petters, M., Suda, S., Guo, H., Weber, R. and Carlton, A.: Trends in particle-phase liquid water during the Southern Oxidant and Aerosol Study, Atmos. Chem. Phys., 14, 10911-10930, 2014.

Orsini, D., Wiedensohler, A., Stratmann, F. and Covert, D.: A new volatility tandem differential mobility analyzer to measure the volatile sulfuric acid aerosol fraction, J. Atmos. Ocean. Technol., 16, 760-772, 1999.

Pachauri, R. K., Allen, M., Barros, V., Broome, J., Cramer, W., Christ, R., Church, J., Clarke, L., Dahe, Q. and Dasgupta, P.: Climate Change 2014: Synthesis Report. Contribution of Working Groups I, II and III to the Fifth Assessment Report of the Intergovernmental Panel on Climate Change, 2014.

Pajunoja, A., Lambe, A. T., Hakala, J., Rastak, N., Cummings, M. J., Brogan, J. F., Hao, L., Paramonov, M., Hong, J. and Prisle, N. L., Malila, J., Romakkaniemi, S., Lehtinen, K.E.J., Laaksonen, A., Kulmala, M., Massoli, P., Onasch, T., Donahue, N., Riipinen, I., Davidovits, P., Worsnop, D.R., Petäjä, T. and Virtanen A.: Adsorptive uptake of water by semisolid secondary organic aerosols, Geophys. Res. Lett., 42, 3063-3068, 2015.

Pajunoja, A., Malila, J., Hao, L., Joutsensaari, J., Lehtinen, K. E. and Virtanen, A.: Estimating the viscosity range of SOA particles based on their coalescence time, Aerosol Science and Technology, 48, i-iv, 2014.

Pajunoja, A., Hu, W., Leong, Y. J., Taylor, N. F., Miettinen, P., Palm, B. B., Mikkonen, S., Collins, D. R., Jimenez, J. L. and Virtanen, A.: Phase state of ambient aerosol linked with water uptake and chemical aging in the southeastern US, Atmos. Chem. Phys., 16, 11163-11176, 2016.

Paramonov, M., Aalto, P., Asmi, A., Prisle, N., Kerminen, V., Kulmala, M. and Petäjä, T.: The analysis of size-segregated cloud condensation nuclei counter (CCNc) data and its implications for cloud droplet activation, Atmos. Chem. Phys., 13, 10285-10301, 2013.

Pathak, R. K., Presto, A. A., Lane, T. E., Stanier, C. O., Donahue, N. M. and Pandis, S. N.: Ozonolysis of alpha-pinene: parameterization of secondary organic aerosol mass fraction, Atmos. Chem. Phys., 7, 3811-3821, 2007.

Perraud, V., Bruns, E. A., Ezell, M. J., Johnson, S. N., Yu, Y., Alexander, M. L., Zelenyuk, A., Imre, D., Chang, W. L. and Dabdub, D.: Nonequilibrium atmospheric secondary organic aerosol formation and growth, Proceedings of the National Academy of Sciences, 109, 2836-2841, 2012.

Peters, A., Wichmann, H., Tuch, T., Heinrich, J. and Heyder, J.: Respiratory effects are associated with the number of ultrafine particles, Am. J. Respir. Crit. Care Med., 155, 1376-1383, 1997.

Petters, M. D., Carrico, C. M., Kreidenweis, S. M., Prenni, A. J., DeMott, P. J., Collett, J. L. and Moosmüller, H.: Cloud condensation nucleation activity of biomass burning aerosol, Journal of Geophysical Research: Atmospheres (1984–2012), 114, 2009.

Petters, M. and Kreidenweis, S.: A single parameter representation of hygroscopic growth and cloud condensation nucleus activity, Atmos. Chem. Phys., 7, 1961-1971, 2007.

Pohlker, C., Wiedemann, K. T., Sinha, B., Shiraiwa, M., Gunthe, S. S., Smith, M., Su, H., Artaxo, P., Chen, Q., Cheng, Y., Elbert, W., Gilles, M. K., Kilcoyne, A. L., Moffet, R. C., Weigand, M., Martin, S. T., Poschl, U. and Andreae, M. O.: Biogenic potassium salt particles as seeds for secondary organic aerosol in the Amazon, Science, 337, 1075-1078, 2012.

Pöschl, U.: Atmospheric aerosols: Composition, transformation, climate and health effects, Angew. Chem. -Int. Edit., 44, 7520-7540, 2005.

Power, R., Simpson, S., Reid, J. and Hudson, A.: The transition from liquid to solid-like behaviour in ultrahigh viscosity aerosol particles, Chem. Sci., 4, 2597-2604, 2013.

Price, H., Murray, B., Mattsson, J., O'Sullivan, D., Wilson, T., Baustian, K. and Benning, L.: Quantifying water diffusion in high-viscosity and glassy aqueous solutions using a Raman isotope tracer method, Atmos. Chem. Phys., 14, 3817-3830, 2014.

Raatikainen, T., Vaattovaara, P., Tiitta, P., Miettinen, P., Rautiainen, J., Ehn, M., Kulmala, M., Laaksonen, A. and Worsnop, D. R.: Physicochemical properties and origin of organic groups detected in boreal forest using an aerosol mass spectrometer, Atmos. Chem. Phys., 10, 2063-2077, 2010.

Rader, D. and McMurry, P.: Application of the Tandem Differential Mobility Analyzer to Studies of Droplet Growth Or Evaporation, J. Aerosol Sci., 17, 771-787, 1986.

Ramanathan, V., Crutzen, P. J., Kiehl, J. T. and Rosenfeld, D.: Aerosols, climate, and the hydrological cycle, Science, 294, 2119-2124, 2001.

Renbaum-Wolff, L., Grayson, J. W., Bateman, A. P., Kuwata, M., Sellier, M., Murray, B. J., Shilling, J. E., Martin, S. T. and Bertram, A. K.: Viscosity of alpha-pinene secondary organic material and implications for particle growth and reactivity, Proc. Natl. Acad. Sci. U. S. A., 110, 8014-8019, 2013.

Riipinen, I., Pierce, J., Yli-Juuti, T., Nieminen, T., Häkkinen, S., Ehn, M., Junninen, H., Lehtipalo, K., Petäjä, T. and Slowik, J.: Organic condensation: a vital link connecting aerosol formation to cloud condensation nuclei (CCN) concentrations, Atmos. Chem. Phys, 11, 3865-3878, 2011.

Riipinen, I., Yli-Juuti, T., Pierce, J. R., Petäjä, T., Worsnop, D. R., Kulmala, M. and Donahue, N. M.: The contribution of organics to atmospheric nanoparticle growth, Nat. Geosci., 5, 453-458, 2012.

Roberts, G. and Nenes, A.: A continuous-flow streamwise thermal-gradient CCN chamber for atmospheric measurements, Aer. Sci. Tech., 39, 206-221, 2005.

Rosati, B., Gysel, M., Rubach, F., Mentel, T. F., Goger, B., Poulain, L., Schlag, P., Miettinen, P., Pajunoja, A., Virtanen, A., Baltink, H. K., Henzing, J. S. B., Gross, J., Gobbi, G. P., Wiedensohler, A., Kiendler-Scharr, A., Decesari, S., Facchini, M. C., Weingartner, E. and Baltensperger, U.: Vertical profiling of aerosol hygroscopic properties in the planetary boundary layer during the PEGASOS campaigns, Atmos. Chem. Phys., 16, 7295-7315, 2016.

Ruehl, C. R., Chuang, P. Y., Nenes, A., Cappa, C. D., Kolesar, K. R. and Goldstein, A. H.: Strong evidence of surface tension reduction in microscopic aqueous droplets, Geophys. Res. Lett., 39, L23801, 2012.

Saha, P. K. and Grieshop, A. P.: Exploring Divergent Volatility Properties from Yield and Thermodenuder Measurements of Secondary Organic Aerosol from alpha-Pinene Ozonolysis, Environ. Sci. Technol., 50, 5740-5749, 2016.

Saha, P. K., Khlystov, A. and Grieshop, A. P.: Determining Aerosol Volatility Parameters Using a "Dual Thermodenuder" System: Application to Laboratory-Generated Organic Aerosols, Aer. Sci. Tech., 49, 620-632, 2015.

Saukko, E., Kuuluvainen, H. and Virtanen, A.: A method to resolve the phase state of aerosol particles, Atmos. Meas. Techn., 5, 259-265, 2012.

Saukko, E., Lambe, A., Massoli, P., Koop, T., Wright, J., Croasdale, D., Pedernera, D., Onasch, T., Laaksonen, A. and Davidovits, P.: Humidity-dependent phase state of SOA particles from biogenic and anthropogenic precursors, Atmos. Chem. Phys., 12, 7517-7529, 2012.

Saukko, E., Zorn, S., Kuwata, M., Keskinen, J. and Virtanen, A.: Phase State and Deliquescence Hysteresis of Ammonium-Sulfate-Seeded Secondary Organic Aerosol, Aer. Sci. Tech., 49, 531-537, 2015.

Saxena, P., Hildemann, L. M., McMurry, P. H. and Seinfeld, J. H.: Organics alter hygroscopic behavior of atmospheric particles, J. Geophys. Res.: Atmospheres, 100, 18755-18770, 1995.

Scott, C., Spracklen, D., Pierce, J., Riipinen, I., D'Andrea, S., Rap, A., Carslaw, K., Forster, P., Artaxo, P. and Kulmala, M.: Impact of gas-to-particle partitioning approaches on the simulated radiative effects of biogenic secondary organic aerosol, Atmos. Chem. Phys., 15, 12989-13001, 2015.

Seinfeld, J. and Pandis, S.: Atmos. Chem. Phys., A Wiley-Inter Science Publication, 2006.

Shiraiwa, M., Pfrang, C., Koop, T. and Pöschl, U.: Kinetic multi-layer model of gas-particle interactions in aerosols and clouds (KM-GAP): linking condensation, evaporation and chemical reactions of organics, oxidants and water, Atmos. Chem. Phys., 12, 2777-2794, 2012.

Shiraiwa, M., Ammann, M., Koop, T. and Pöschl, U.: Gas uptake and chemical aging of semisolid organic aerosol particles, Proc. Natl. Acad. Sci. U. S. A., 108, 11003-11008, 2011.

Shiraiwa, M., Yee, L. D., Schilling, K. A., Loza, C. L., Craven, J. S., Zuend, A., Ziemann, P. J. and Seinfeld, J. H.: Size distribution dynamics reveal particle-phase chemistry in organic aerosol formation, Proc. Natl. Acad. Sci. U. S. A., 110, 11746-11750, 2013.

Shiraiwa, M. and Seinfeld, J. H.: Equilibration timescale of atmospheric secondary organic aerosol partitioning, Geophys. Res. Lett., 39, L24801, 2012.

Shiraiwa, M., Zuend, A., Bertram, A. K. and Seinfeld, J. H.: Gas-particle partitioning of atmospheric aerosols: interplay of physical state, non-ideal mixing and morphology, Phys. Chem. Chem. Phys., 15, 11441-11453, 2013.

Shrivastava, M., Zelenyuk, A., Imre, D., Easter, R., Beranek, J., Zaveri, R. A. and Fast, J.: Implications of low volatility SOA and gas-phase fragmentation reactions on SOA loadings and their spatial and temporal evolution in the atmosphere, J. Geophys Res: Atmospheres, 118, 3328-3342, 2013.

Smith, M., Bertram, A. and Martin, S.: Deliquescence, efflorescence, and phase miscibility of mixed particles of ammonium sulfate and isoprene-derived secondary organic material, Atmos. Chem. Phys., 12, 9613-9628, 2012.

Song, M., Liu, P., Hanna, S., Li, Y., Martin, S. and Bertram, A.: Relative humidity-dependent viscosities of isoprene-derived secondary organic material and atmospheric implications for isoprene-dominant forests, Atmos. Chem. Phys., 15, 5145-5159, 2015.

Sorjamaa, R. and Laaksonen, A.: The effect of H 2 O adsorption on cloud drop activation of insoluble particles: a theoretical framework, Atmos. Chem. Phys., 7, 6175-6180, 2007.

Spracklen, D. V., Carslaw, K. S., Merikanto, J., Mann, G. W., Reddington, C. L., Pickering, S., Ogren, J. A., Andrews, E., Baltensperger, U., Weingartner, E., Boy, M., Kulmala, M., Laakso, L., Lihavainen, H., Kivekas, N., Komppula, M., Mihalopoulos, N., Kouvarakis, G., Jennings, S. G., O'Dowd, C., Birmili, W., Wiedensohler, A., Weller, R., Gras, J., Laj, P., Sellegri, K., Bonn, B., Krejci, R., Laaksonen, A., Hamed, A., Minikin, A., Harrison, R. M., Talbot, R. and Sun, J.: Explaining global surface aerosol number concentrations in terms of primary emissions and particle formation, Atmos. Chem. Phys., 10, 4775-4793, 2010.

Stocker, T., Qin, D., Plattner, G., Tignor, M., Allen, S. K., Boschung, J., Nauels, A., Xia, Y., Bex, V. and Midgley, P. M.: Climate change 2013: The physical science basis, Cambridge University Press Cambridge, UK, and New York, 2014.

Sumner A. L., Menke, E., Dubowski, Y., Newberg, J. T., Penner, R. M., Hemminger, J. C., Wingen, L. M., Brauers, T., and Finlayson-Pitts, B. J., The nature of water on surfaces of laboratory systems and implications for heterogeneous chemistry in the troposphere, Phys. Chem. Chem. Phys. 6, 604-614, 2004.

Svenningsson, I., Hansson, H., Wiedensohler, A., Ogren, J., Noone, K. and Hallberg, A.: Hygroscopic growth of aerosol particles in the Po Valley, Tellus B, 44, 556-569, 1992.

Swietlicki, E., Hansson, H., Hämeri, K., Svenningsson, B., Massling, A., McFiggans, G., McMurry, P., Petäjä, T., Tunved, P. and Gysel, M.: Hygroscopic properties of submicrometer atmospheric aerosol particles measured with H-TDMA instruments in various environments - A review, Tellus B, 60, 432-469, 2008.

Tadros, ME, HU P and Adamson A.W., Adsorption and contact angle studies I. Water on smooth carbon, linear polyethylene, and stearic acid coated copper, J. Colloid Interface Sci. 49, 184-195, 1974.

Thomson, W.: On the equilibrium of vapour at a curved surface of liquid, Philosophical Magazine, series 4, 42 (282), 448-452, 1871.

Tong, H., Reid, J., Bones, D., Luo, B. and Krieger, U.: Measurements of the timescales for the mass transfer of water in glassy aerosol at low relative humidity and ambient temperature, Atmos. Chem. Phys., 11, 4739-4754, 2011.

Topping, D., McFiggans, G. and Coe, H.: A curved multi-component aerosol hygroscopicity model framework: Part 2–Including organic compounds, Atmos. Chem. Phys., 5, 1223-1242, 2005.

Tritscher, T., Dommen, J., DeCarlo, P., Gysel, M., Barmet, P., Praplan, A., Weingartner, E., Prévôt, A., Riipinen, I. and Donahue, N.: Volatility and hygroscopicity of aging secondary organic aerosol in a smog chamber, Atmos. Chem. Phys., 11, 11477-11496, 2011.

Twomey, S.: The composition of cloud nuclei, J. Atmos. Sci., 28, 377-381, 1971.

Vaden, T. D., Imre, D., Beranek, J., Shrivastava, M. and Zelenyuk, A.: Evaporation kinetics and phase of laboratory and ambient secondary organic aerosol, Proc. Natl. Acad. Sci. U. S. A., 108, 2190-2195, 2011.

Virtanen, A., Kannosto, J., Kuuluvainen, H., Arffman, A., Joutsensaari, J., Saukko, E., Hao, L., Yli-Pirilä, P., Tiitta, P. and Holopainen, J.: Bounce behavior of freshly nucleated biogenic secondary organic aerosol particles, Atmos. Chem. Phys., 11, 8759-8766, 2011.

Virtanen, A., Joutsensaari, J., Koop, T., Kannosto, J., Yli-Pirilä, P., Leskinen, J., Mäkelä, J. M., Holopainen, J. K., Pöschl, U. and Kulmala, M.: An amorphous solid state of biogenic secondary organic aerosol particles, Nature, 467, 824-827, 2010.

Wang, B., O'Brien, R. E., Kelly, S. T., Shilling, J. E., Moffet, R. C., Gilles, M. K. and Laskin, A.: Reactivity of Liquid and Semisolid Secondary Organic Carbon with Chloride and Nitrate in Atmospheric Aerosols, J. Phys. Chem. A, 119, 4498-4508, 2015.

Went, F. W.: Blue hazes in the atmosphere, Nature, 187, 641-643, 1960.

Wex, H., Petters, M., Carrico, C., Hallbauer, E., Massling, A., McMeeking, G., Poulain, L., Wu, Z., Kreidenweis, S. and Stratmann, F.: Towards closing the gap between hygroscopic growth and activation for secondary organic aerosol: Part 1–Evidence from measurements, Atmos. Chem. Phys., 9, 3987-3997, 2009.

Wilson J., Imre D., Beranek J., Shrivastava M. and Zelenyuk. A.: Evaporation Kinetics of Laboratory-Generated Secondary Organic Aerosols at Elevated Relative Humidity, Environ. Sci. Tech. 49, 243-249, 2015.

Xu, L., Guo, H., Boyd, C. M., Klein, M., Bougiatioti, A., Cerully, K. M., Hite, J. R., Isaacman-VanWertz, G., Kreisberg, N. M., Knote, C., Olson, K., Koss, A., Goldstein, A. H., Hering, S. V., de Gouw, J., Baumann, K., Lee, S. H., Nenes, A., Weber, R. J. and Ng, N. L.: Effects of anthropogenic emissions on aerosol formation from isoprene and monoterpenes in the southeastern United States, Proc. Natl. Acad. Sci. U. S. A., 112, 37-42, 2015.

Zaveri, R. A., Easter, R. C., Shilling, J. E. and Seinfeld, J.: Modeling kinetic partitioning of secondary organic aerosol and size distribution dynamics: representing effects of volatility, phase state, and particle-phase reaction, Atmos. Chem. Phys., 14, 5153-5181, 2014.

Zaveri, R. A., Shaw, W. J., Cziczo, D. J., Schmid, B., Ferrare, R. A., Alexander, M. L., Alexandrov, M., Alvarez, R. J., Arnott, W. P., Atkinson, D. B., Baidar, S., Banta, R. M., Barnard, J. C., Beranek, J., Berg, L. K., Brechtel, F., Brewer, W. A., Cahill, J. F., Cairns, B., Cappa, C. D., Chand, D., China, S., Comstock, J. M., Dubey, M. K., Easter, R. C., Erickson, M. H., Fast, J. D., Floerchinger, C., Flowers, B. A., Fortner, E., Gaffney, J. S., Gilles, M. K., Gorkowski, K., Gustafson, W. I., Gyawali, M., Hair, J., Hardesty, R. M., Harworth, J. W., Herndon, S., Hiranuma, N., Hostetler, C., Hubbe, J. M., Jayne, J. T., Jeong, H., Jobson, B. T., Kassianov, E. I., Kleinman, L. I., Kluzek, C., Knighton, B., Kolesar, K. R.,

Kuang, C., Kubatova, A., Langford, A. O., Laskin, A., Laulainen, N., Marchbanks, R. D., Mazzoleni, C., Mei, F., Moffet, R. C., Nelson, D., Obland, M. D., Oetjen, H., Onasch, T. B., Ortega, I., Ottaviani, M., Pekour, M., Prather, K. A., Radney, J. G., Rogers, R. R., Sandberg, S. P., Sedlacek, A., Senff, C. J., Senum, G., Setyan, A., Shilling, J. E., Shrivastava, M., Song, C., Springston, S. R., Subramanian, R., Suski, K., Tomlinson, J., Volkamer, R., Wallace, H. W., Wang, J., Weickmann, A. M., Worsnop, D. R., Yu, X. -., Zelenyuk, A. and Zhang, Q.: Overview of the 2010 Carbonaceous Aerosols and Radiative Effects Study (CARES), Atmos. Chem. Phys., 12, 7647-7687, 2012.

Zhang, Y., Sanchez, M., Douet, C., Wang, Y., Bateman, A., Gong, Z., Kuwata, M., Renbaum-Wolff, L., Sato, B. and Liu, P., Bertram, A.K., Geiger, F.M., Martin, S.T.: Changing shapes and implied viscosities of suspended submicron particles, Atmos. Chem. Phys., 15, 7819-7829, 2015.

Zobrist, B., Soonsin, V., Luo, B. P., Krieger, U. K., Marcolli, C., Peter, T. and Koop, T.: Ultra-slow water diffusion in aqueous sucrose glasses, Phys. Chem. Chem. Phys., 13, 3514-3526, 2011.

Zobrist, B., Marcolli, C., Pedernera, D. A. and Koop, T.: Do atmospheric aerosols form glasses?, Atmos. Chem. Phys., 8, 5221-5244, 2008.